


ARTICLE

# Lymphocyte egress signal sphingosine-1-phosphate promotes ERM-guided, bleb-based migration

Tanner F. Robertson<sup>1,2</sup> , Pragati Chengappa<sup>3</sup> , Daniela Gomez Atria<sup>4</sup> , Christine F. Wu<sup>1,2</sup>, Lyndsay Avery<sup>1,2</sup> , Nathan H. Roy<sup>1,2</sup> , Ivan Maillard<sup>4</sup>, Ryan J. Petrie<sup>3</sup> , and Janis K. Burkhardt<sup>1,2</sup> 

**Ezrin, radixin, and moesin (ERM) family proteins regulate cytoskeletal responses by tethering the plasma membrane to the underlying actin cortex. Mutations in ERM proteins lead to severe combined immunodeficiency, but the function of these proteins in T cells remains poorly defined. Using mice in which T cells lack all ERM proteins, we demonstrate a selective role for these proteins in facilitating S1P-dependent egress from lymphoid organs. ERM-deficient T cells display defective S1P-induced migration in vitro, despite normal responses to standard protein chemokines. Analysis of these defects revealed that S1P promotes a fundamentally different mode of migration than chemokines, characterized by intracellular pressurization and bleb-based motility. ERM proteins facilitate this process, controlling directional migration by limiting blebbing to the leading edge. We propose that the distinct modes of motility induced by S1P and chemokines are specialized to allow T cell migration across lymphatic barriers and through tissue stroma, respectively.**

## Introduction

Adaptive immunity depends on the ability of lymphocytes to effectively survey the body for cognate antigen. To achieve this, lymphocytes perpetually traffic into, within, and out of secondary lymphoid organs by a process that depends on the integrated function of multiple cytoskeletal regulatory proteins. Ezrin, radixin, and moesin (ERM) family proteins are highly homologous cytoskeletal organizers that form a regulated linkage between the plasma membrane (PM) and underlying actin cortex (Fehon et al., 2010). Expression of constitutively active ERM mutants disrupts cytoskeletal responses and dysregulates lymphocyte trafficking (Liu et al., 2012; Martinelli et al., 2013; Parameswaran et al., 2011). Moreover, hemizygous mutations in moesin cause severe combined immunodeficiency in humans, a disease characterized by sharp declines in circulating lymphocytes and recurrent infections (Lagresle-Peyrou et al., 2016). While constitutively active ERM proteins potentially interfere with lymphocyte behavior, their effects are pleiotropic, making it difficult to ascertain the normal function of endogenous proteins. Importantly, loss-of-function approaches yield much milder phenotypes. In the absence of ERM proteins, lymphocytes polarize, migrate, and chemotax normally in most situations (Chen et al., 2013). Because T cells express both ezrin

and moesin, functional redundancy likely contributes to the mild phenotype of cells lacking only one isoform, but the extent of functional compensation is unclear. As a result, the normal physiological role for ERM proteins in lymphocyte trafficking has remained obscure.

Here, we overcome these challenges using a new mouse model in which mature T cells lack all ERM proteins. In these mice, we find that ERM proteins are preferentially required for egress from lymphoid organs, a process driven by the signaling lipid sphingosine-1-phosphate (S1P; Allende et al., 2004; Matloubian et al., 2004). The migratory response to S1P that mediates egress is poorly understood. Using an optimized approach, we find that S1P elicits a fundamentally different mode of migration from that induced by protein chemokines. Whereas chemokine-induced migration utilizes actin-rich lamellipodial protrusions, S1P drives intracellular pressurization and polarized membrane blebbing, a distinct mode of motility. While dispensable for lamellipodial responses, ERM proteins play a critical role in guiding bleb-based motility in response to S1P. These findings yield novel insights into the mechanism of lymphocyte egress and provide a framework for understanding ERM-associated immune dysfunction.

<sup>1</sup>Department of Pathology and Laboratory Medicine, Children’s Hospital of Philadelphia Research Institute, Philadelphia, PA; <sup>2</sup>Perelman School of Medicine, University of Pennsylvania, Philadelphia, PA; <sup>3</sup>Department of Biology, Drexel University, Philadelphia, PA; <sup>4</sup>Division of Hematology-Oncology, Department of Medicine, Abramson Family Cancer Research Institute, University of Pennsylvania Perelman School of Medicine, Philadelphia, PA.

Correspondence to Janis K. Burkhardt: [jburkhar@penmedicine.upenn.edu](mailto:jburkhar@penmedicine.upenn.edu).

© 2021 Robertson et al. This article is distributed under the terms of an Attribution–Noncommercial–Share Alike–No Mirror Sites license for the first six months after the publication date (see <http://www.rupress.org/terms/>). After six months it is available under a Creative Commons License (Attribution–Noncommercial–Share Alike 4.0 International license, as described at <https://creativecommons.org/licenses/by-nc-sa/4.0/>).



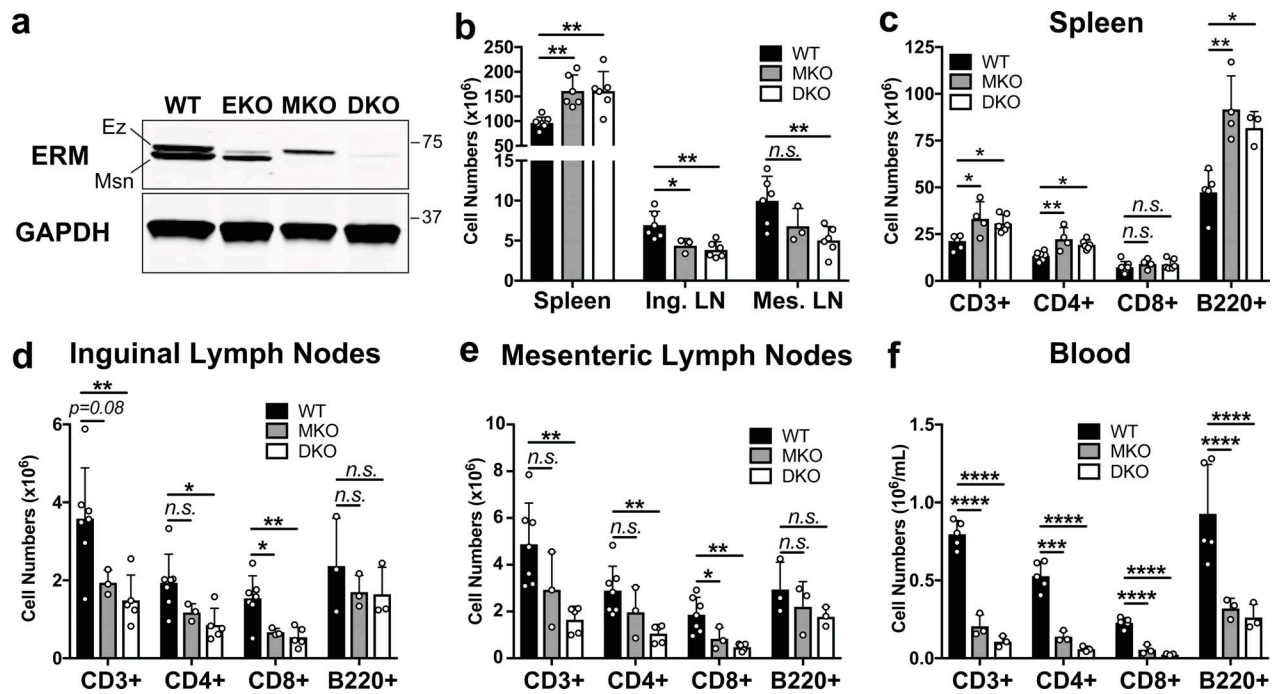


Figure 1. **ERM-deficient lymphocytes assume an altered tissue distribution with severe lymphopenia.** (a) Lysates from CD4<sup>+</sup> T cell blasts were immunoblotted with a pan-ERM antibody and anti-GAPDH. (b) Total cell counts from spleens (after RBC lysis), inguinal lymph nodes (Ing. LN), and mesenteric lymph nodes (Mes. LN) from 8–16-wk-old mice. (c–f) Cell suspensions and peripheral blood mononuclear cells were analyzed by flow cytometry. (b–f) Data represent means ± SD. Each dot represents an individual mouse; n = 3–7 mice per group. Statistical significance was determined using a standard one-way ANOVA. Data distribution was assumed to be normal, but this was not formally tested. Ez, ezrin; Msn, moesin. n.s., P > 0.05; \*, P < 0.05; \*\*, P < 0.01; \*\*\*, P < 0.001; \*\*\*\*, P < 0.0001.

## Results

### ERM-deficient lymphocytes show an altered distribution among lymphoid organs and blood

Members of the ERM protein family are highly homologous and often display functional overlap when coexpressed (Fehon et al., 2010). Since T cells express high levels of both moesin and ezrin, we generated germline moesin knockout mice (MKO) by targeted disruption of the *Msn* gene (Fig. S1) and crossed them to mice with a conditional deletion of *Ezn* in the T cell compartment (ezrin<sup>Fl/Fl</sup>;CD4<sup>Cre</sup> [EKO]; Shaffer et al., 2009) to generate animals in which mature T cells lack both gene products (double knockout [DKO]). Western blot analysis of CD4<sup>+</sup> T cells confirmed that ezrin and moesin were eliminated as expected; radixin levels remained low (Fig. 1 a). Note that B cells in both MKO and DKO mice lack moesin but continue to express ezrin. Mice were born at Mendelian frequencies and were grossly indistinguishable from WT littermates. Histological analysis did not reveal overt pathology or aberrant accumulation of leukocytes in nonlymphoid organs (skin, liver, and kidney, collected at 8–16 wk of age; data not shown).

Analysis of secondary lymphoid organs from both MKO and DKO mice revealed marked alterations in lymphocyte distribution. Spleens were enlarged compared with WT mice (Fig. S2, a–c) and showed elevated cellularity and lymphocyte numbers (Fig. 1, b and c), while inguinal and mesenteric lymph nodes showed diminished total cellularity and T cell numbers (Fig. 1, d, and e). Numbers of lymph node B cells were also reduced, although this did not reach statistical significance. Despite these alterations, ERM-deficient lymphocytes generally segregated

into the correct anatomical locations within the spleens and lymph nodes, although the organization of these zones was more diffuse than in WT mice (Fig. S2, b–h). Most strikingly, MKO and DKO mice displayed sharp reductions in the numbers of all lymphocytes in the blood (Fig. 1 f). Overall, the phenotypes of MKO and DKO mice were similar, but DKO mice consistently exhibited more pronounced defects. This likely reflects the fact that moesin is the more abundant isoform in T cells, and indicates that some functional redundancy exists between ezrin and moesin in this setting. Given the more profound defects in DKO mice, only these animals were used for further experiments.

Within the thymi of DKO mice, double-negative and double-positive thymocytes appeared in normal numbers and frequency, indicating that loss of ezrin and moesin does not result in gross perturbations in T cell development (Fig. 2, a and b). CD4 and CD8 single-positive populations showed a mild increase; further analysis demonstrated that this was due to a significant accumulation of mature (CD24<sup>low</sup>, SIPR1<sup>hi</sup>) single-positive thymocytes (Fig. 2, c–f). This phenotype and the peripheral lymphopenia we observe (Fig. 1 f) are common features of mice exhibiting defects in egress from lymphoid organs (Allende et al., 2004; Matloubian et al., 2004). Taken together, these data suggest that ERM proteins are important for homeostatic lymphocyte trafficking.

### ERM deficiency results in cell-intrinsic defects in egress from lymphoid organs

To ask if the altered distribution of ERM-deficient lymphocytes reflects a cell-intrinsic trafficking defect, we performed competitive

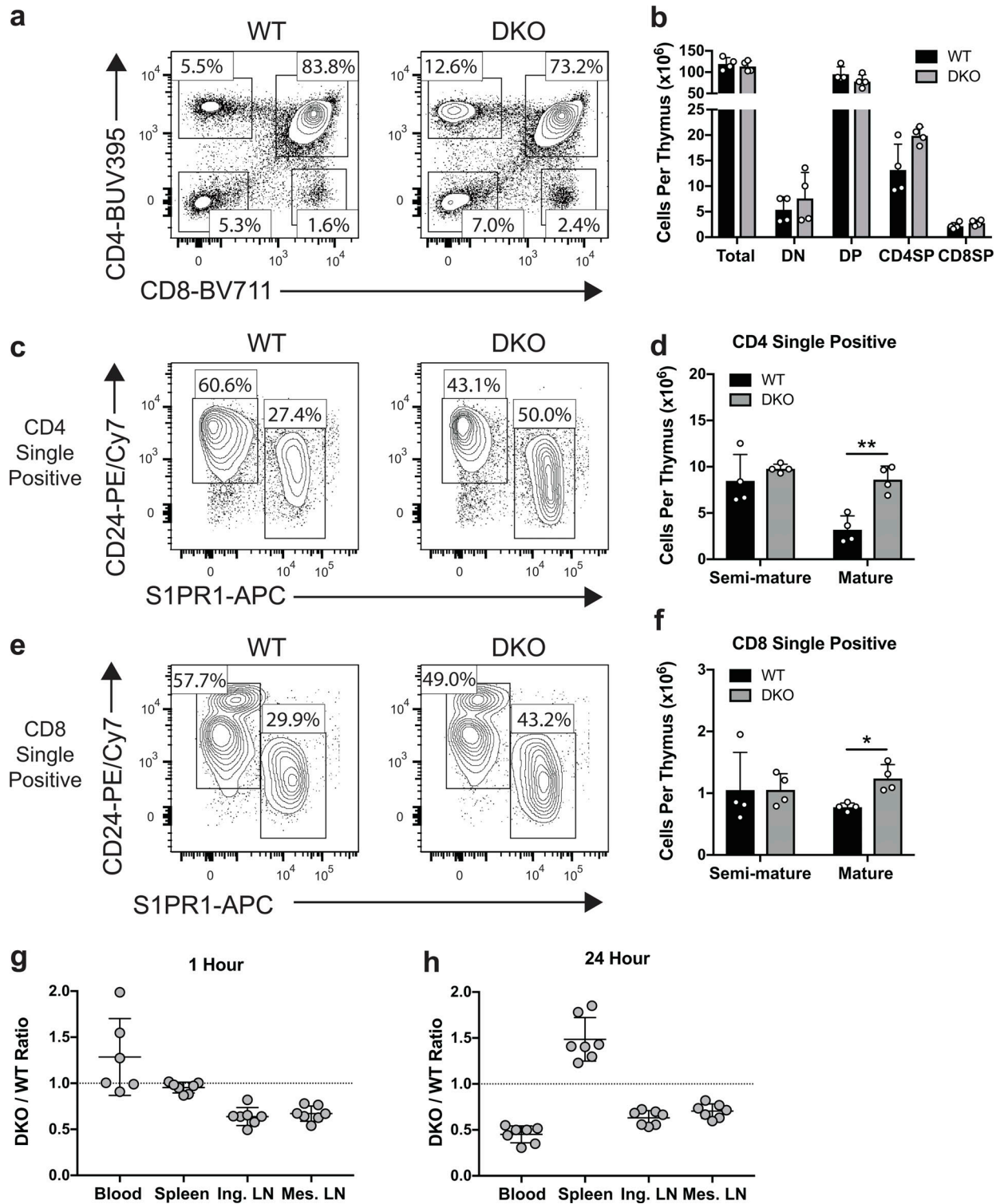


Figure 2. **ERM-deficient T cells have a cell-intrinsic egress defect.** (a and b) Representative flow plots and total numbers of major thymocyte populations. (c–f) CD4 single-positive (c and d) and CD8 single-positive (e and f) populations were analyzed to determine the numbers of semi-mature (CD24<sup>hi</sup>S1PR1<sup>low</sup>) and mature (CD24<sup>low</sup>S1PR1<sup>hi</sup>) subpopulations. (e and f) Statistical significance for b, d, and f was determined by comparing the WT and DKO means using multiple t tests (two-sided) and the Holm-Sidak correction for multiple comparisons. Each dot represents an individual mouse; *n* = 4. Data distribution was assumed to be normal, but this was not formally tested. (g and h) Competitive in vivo migration. CD45 congenic WT and DKO naive CD4<sup>+</sup> T cells labeled with CFMFA were coinjected 1:1 into the tail veins of WT recipient mice and harvested from the indicated tissues 1 or 24 h later. Each dot represents a recipient mouse; data are pooled from two independent experiments. Means ± SD are indicated with horizontal bars in d, f, g, and h. Dotted lines in g and h indicate a 1:1 ratio. DN, double negative; DP, double positive; SP, single positive; Ing. LN, inguinal lymph node; Mes. LN, mesenteric lymph node. \*, *P* < 0.05; \*\*, *P* < 0.01.

in vivo migration assays by labeling naive CD4<sup>+</sup> T cells from DKO mice and congenically marked WT controls with cell tracking dyes and coinjecting them into the lateral tail veins of WT recipients. To distinguish between entry and egress defects, cells were analyzed 1 h after injection, when egress is minimal, and 24 h after injection, when trafficking reaches equilibrium (Mandl et al., 2012; Smith and Ford, 1983). At 1 h, DKO T cells showed a 30–40% reduction in lymph node entry and a corresponding elevation in the blood (Fig. 2 g). This points to a role for ERM proteins in promoting T cell passage into lymph nodes across high endothelial venules. Entry into the spleen, which occurs via an open system continuous with blood (Grayson et al., 2003; Lyons and Parish, 1995), was equally efficient for WT and DKO T cells. By 24 h, DKO T cells accumulated in the spleen and showed a corresponding decrease in the blood (Fig. 2 h), consistent with a defect in splenic egress. The relative paucity of DKO T cells in lymph nodes was maintained from 1 to 24 h after injection, most likely because the reduced entry rate evident at 1 h is matched by a reduced lymph node egress rate (Mandl et al., 2012). Importantly, the distribution of transferred T cells at 24 h matched the altered tissue distribution observed in the DKO mice (Fig. 1, b–f), indicating that the observed alterations in the DKO mice are T cell intrinsic. Taken together, these studies show that although loss of ERM proteins impairs both entry and egress from lymphoid organs, the egress defects drive the most profound phenotypes, including accumulation of mature thymocytes, splenomegaly, and severe peripheral lymphopenia. Thus, we focused on understanding the molecular basis for this egress defect.

### ERM proteins are selectively required for S1P-induced migratory responses

The central signal that governs lymphocyte egress is S1P, a pleiotropic signaling lipid that is rich in blood and lymph but low in interstitial fluids of lymphoid organs (Schwab et al., 2005; Yatomi et al., 1997). T cells recognize S1P through the receptor S1PR1 (*Edg1*), which prompts egress (Allende et al., 2004; Cyster and Schwab, 2012; Grigorova et al., 2009; Matloubian et al., 2004). Our initial attempts to study S1P-induced migration of WT and DKO T cells were stymied by the fact that T cells are notoriously unresponsive to S1P in vitro (Arnon et al., 2011; Willinger et al., 2014), a problem that is further complicated by the presence of S1P in cell culture serum. In other cell types, optimal S1P responses can be achieved by overnight culture in serum-free media (Gandy et al., 2013), but this strategy results in unacceptable levels of death for primary T cells. To maintain T cell viability, we used charcoal-stripped FBS (CS-FBS), which is devoid of lipophilic components. T cells cultured overnight in media supplemented with CS-FBS were mostly viable and displayed dramatically enhanced transmigration to S1P relative to freshly isolated cells cultured for 1 h in the same media (Fig. 3 a). Inhibiting S1PR1 with the selective antagonist Ex26 (Cahalan et al., 2013) completely abrogated transmigration, verifying that the response was S1PR1 dependent. This optimized procedure allows for robust functional assays, making it possible to ask fundamental questions about cell biological responses to S1P.

Using this improved in vitro approach, we found that DKO T cells were highly defective in transmigration toward S1P

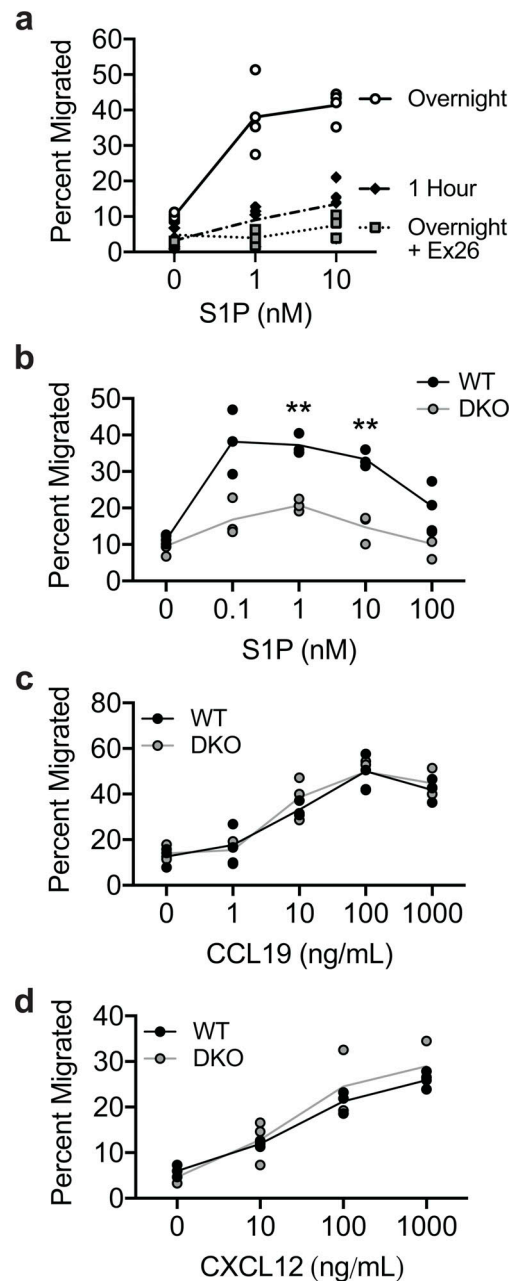


**Figure 3. DKO T cells have a selective transmigration defect toward S1P.** (a) Transmigration to the indicated doses of S1P. Naive CD4<sup>+</sup> T cells cultured for 1 h or overnight in media with CS-FBS, with or without pretreatment with 100 nM Ex26. Each data point represents the mean of technical replicates from one independent experiment ( $n = 4$  experiments). (b–d) Percent transmigration of WT and DKO naive CD4<sup>+</sup> T cells (previously cultured overnight in media with 10% CS-FBS) to the indicated doses of S1P (b), CCL19 (c), or CXCL12 (d). Each data point represents one technical replicate from one experiment, representative of three to five independent experiments. Means for each concentration of chemoattractant were compared with *t* tests (two-sided) using the Holm-Sidak correction for multiple comparisons. Data distribution was assumed to be normal, but this was not formally tested. \*\*,  $P < 0.01$ .

across multiple doses (Fig. 3 b). Remarkably, transmigration toward CCL19 or CXCL12, two chemokines involved in naive T cell trafficking (Bai et al., 2009; Förster et al., 1999), was

entirely normal (Fig. 3, c and d). These data indicate that while ERM proteins are not required for directed T cell migration generally, they are selectively critical for S1P-induced migratory responses.

### ERM proteins are dispensable for S1PR1 expression and endocytosis

We next sought to determine how ERM proteins foster T cell migration in response to S1P. Since cell surface expression of S1PR1 and ligand-induced endocytosis are both known to impact S1P-dependent T cell egress (Allende et al., 2004; Arnon et al., 2011; Matloubian et al., 2004; Willinger et al., 2014), we asked if ERM protein expression is required for these events. Across multiple secondary lymphoid organs, surface S1PR1 levels on naive DKO CD4<sup>+</sup> T cells were normal or slightly elevated (Fig. 4 a). Receptor expression also appeared normal in mature DKO thymocyte populations (Fig. 2, c and e). Additionally, DKO T cells displayed low surface expression of S1PR1 when isolated from blood, a high S1P environment, indicating that receptor endocytosis *in vivo* is intact (Fig. 4 a). To confirm that ERM proteins are dispensable for S1PR1 endocytosis, we treated cells with S1P *in vitro* for 30 s or 10 min, stained for surface S1PR1, and measured loss of receptor expression by flow cytometry. WT and DKO T cells showed similar surface levels of S1PR1 in culture, and no differences were detected in the efficiency or kinetics of endocytosis following S1P treatment (Fig. 4, b and c). Thus, we conclude that receptor expression and ligand-induced internalization are intact.

### ERM proteins are dispensable for S1P-dependent signaling

Since ERM proteins interact with important signaling proteins at the PM (Viswanatha et al., 2013), we asked if DKO T cells show signaling defects downstream of S1PR1 ligation. Studies on S1PR1 signaling in lymphocytes are lacking, but S1PR1 has been shown to signal through the PI3K/Akt and MAPK pathways in other cell types (Mullershausen et al., 2009; Vrzalikova et al., 2018). We stimulated WT and DKO T cells with S1P for various times and immunoblotted for phospho-Akt and phospho-Erk1/2. As shown in Fig. 4 d, the magnitude and kinetics of signaling through both intermediates were similar for WT and DKO T cells. As a separate readout of S1PR1 signaling, we measured actin polymerization. Again, we found no differences in the response of WT and DKO T cells (Fig. 4, e and f). Treatment with Ex26 effectively blocked actin polymerization, confirming the receptor specificity of this response (data not shown). Taken together, these studies show that ERM protein expression is not required for ligand-induced S1PR1 internalization or signaling.

### S1P induces rapid dephosphorylation and rephosphorylation of ERM proteins

Since S1PR1 appeared to be fully signaling-competent in DKO T cells, we considered alternative explanations for the transmigration defects we observed. ERM proteins cycle between an activated conformation at the PM and an auto-inhibited head-to-tail conformation in the cytoplasm (Gary and Bretscher, 1995). Activation is mediated by binding of the N-terminal FERM domain to PIP<sub>2</sub> in the PM and by phosphorylation of a critical

threonine residue in the C-terminal actin-binding domain (Fievet et al., 2004). Chemokine receptor signaling in T cells promotes potent ERM dephosphorylation lasting 10–20 min, during which the cell can undergo shape changes and molecular reorganization events needed for polarized cell motility (Brown et al., 2003; Shaffer et al., 2009). To better understand how ERM proteins function during S1P-mediated motility, we analyzed the cycling of ERM proteins in cells responding to S1P or CCL19. Interestingly, although both CCL19 and S1P induced ERM dephosphorylation at 30 s, dephosphorylation was sustained in CCL19-treated cells whereas S1P-treated cells showed rapid ERM rephosphorylation 2–5 min after stimulation (Fig. 5, a and b).

### S1P induces a rapid, transient mode of motility that depends on ERM proteins

To study the differences between S1P- and chemokine-induced migration, we developed a chemokinesis assay to visualize cell dynamics following chemoattractant stimulation. WT naive CD4<sup>+</sup> T cells were added to chambers coated with vascular adhesion protein-1 (VCAM) and imaged for several minutes at which point S1P, CCL19, or CXCL12 was gently dripped into the chamber. Prior to stimulation, VCAM-bound cells primarily exhibited a rounded morphology. Addition of S1P induced a rapid burst of migration lasting only a few minutes, after which the cells rounded up and stopped moving (Video 1). In contrast, both CCL19 and CXCL12 induced modest but sustained chemokinetic responses (Video 2 and Video 3). Analysis of cell velocity confirmed this distinction; S1P induced strong, but short-lived responses that returned to baseline within 4–5 min, whereas CCL19 and CXCL12 induced sustained migration (Fig. 5 c). These distinct modes of motility are reflected in the kinetics of F-actin polymerization, which is short-lived in S1P-stimulated cells and sustained for at least 20 min in cells treated with CCL19 (Fig. S3). Importantly, during the time when S1P-treated T cells exhibit maximal motility (~2 min after stimulation; Fig. 5 c), ERM protein phosphorylation has already returned to significant levels (Fig. 5, a and b). This contrasts with chemokine-stimulated cells, where phospho-ERM protein levels remain low throughout the migratory period.

We next used this chemokinesis assay to conduct side-by-side analysis of WT and DKO T cells. We first quantified the number of cells that migrate in response to each chemoattractant (defined by displacement of at least 10 μm, roughly 1.5 cell diameters). Similar to the transwell data (Fig. 4, b–d), fewer DKO than WT T cells migrated in response to S1P (Fig. 6 a, Video 1, and Video 4), whereas the frequency of DKO cells migrating to CCL19 and CXCL12 was unaffected (Fig. 6 b). Among the cells that did migrate, DKO T cells showed reduced displacement and directionality in response to S1P (Fig. 6, c and e), but not CCL19 or CXCL12 (Fig. 6, d and f–h).

### S1P induces pressurized, bleb-based migration

During our analysis of T cell dynamics, we observed that although WT cells responding to S1P and chemokines exhibited similar morphologies at early time points, their behavior differed dramatically after the first 2–3 min. Prior to stimulation, cells were rounded and poorly migratory (Fig. 7, a and b, Pre-treat).

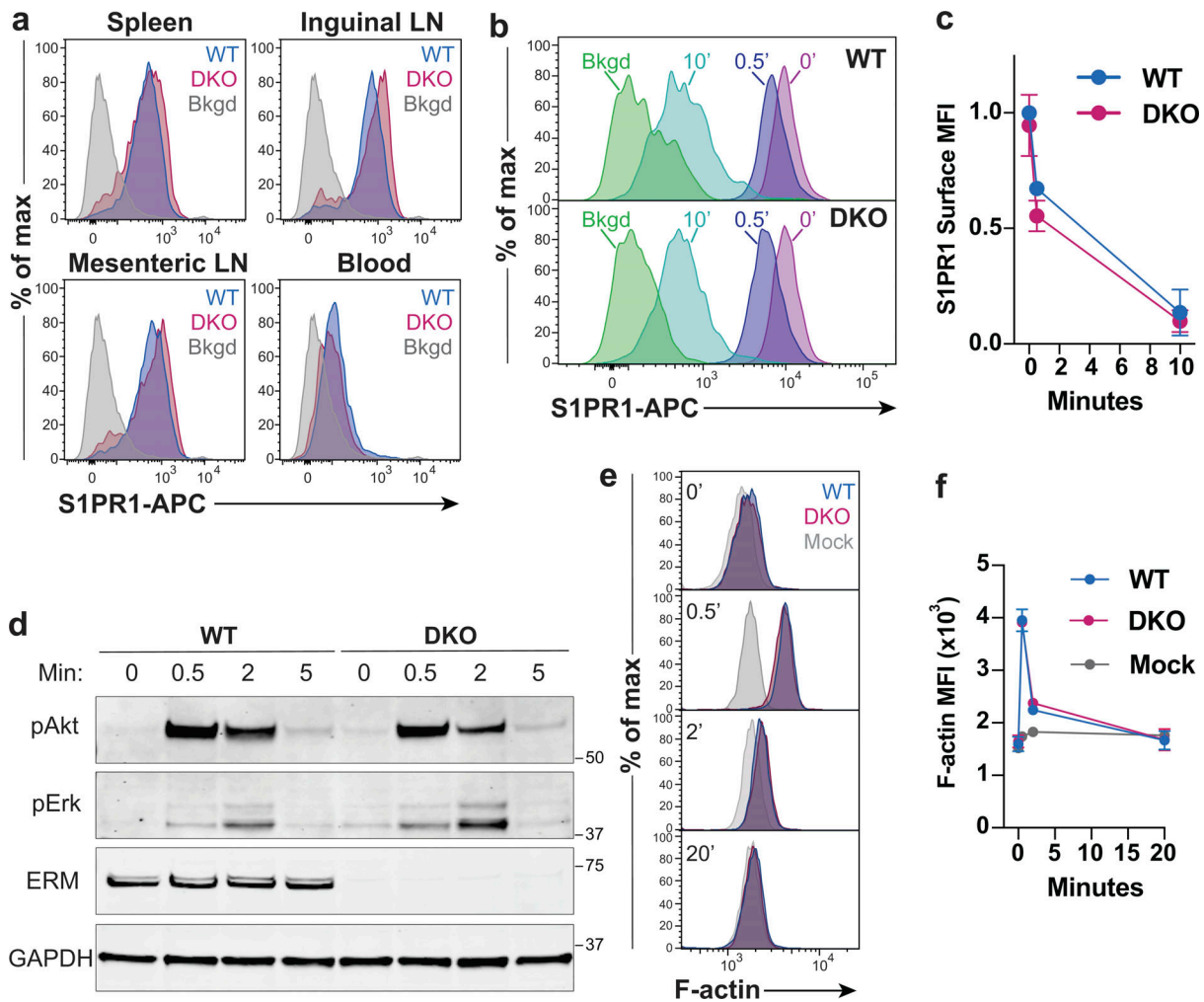


**Figure 4. ERM proteins are dispensable for S1PR1 expression, endocytosis, and signaling.** (a) Ex vivo surface expression of S1PR1 on WT and DKO naive CD4<sup>+</sup> T cells (CD4<sup>+</sup>, CD62L<sup>Hi</sup>, CD44<sup>Low</sup>) from the spleens, lymph nodes (LNs), and blood. Bkgd refers to WT CD4<sup>+</sup>CD8<sup>+</sup> thymocytes stained in parallel. Representative flow panels from three independent experiments are shown. (b and c) Ligand-induced S1PR1 endocytosis. WT and DKO naive CD4<sup>+</sup> T cells were cultured overnight in media with 10% CS-FBS, stimulated with S1P (10 nM) for 0, 0.5, or 10 min, stained for surface S1PR1, and analyzed by flow cytometry. Bkgd refers to cells stained without primary anti-S1PR1 antibody. Pooled data from four independent experiments normalized to WT levels before stimulation are shown as means ± SD and compared at each time point using *t* tests (two-sided) and the Holm-Sidak correction for multiple comparisons. (d) S1P-induced signaling. WT and DKO naive CD4<sup>+</sup> T cells (previously cultured overnight in media with 10% CS-FBS) were stimulated with S1P (1 nM), lysed after 0, 0.5, 2, and 5 min, and immunoblotted for phospho-Erk (pErk; Thr202/Tyr204), phospho-Akt (pAkt; Ser473), total ERM proteins, and GAPDH. The blot shown is representative of three independent experiments. (e and f) S1P-induced actin polymerization. WT and DKO naive CD4<sup>+</sup> T cells (previously cultured overnight in media with 10% CS-FBS) were stimulated with S1P (1 nM) for 0, 0.5, 2, or 20 min, fixed, stained with phalloidin-AF488, and analyzed by flow cytometry. Mock treated cells were handled in parallel, with addition media alone. Representative plots and pooled data from four independent experiments are shown as means ± SD and compared at each time point using multiple *t* tests (two-sided) with the Holm-Sidak correction for multiple comparisons. Data distribution was assumed to be normal, but this was not formally tested. No statistically significant differences were observed between WT and DKO T cell responses. Max, maximum; MFI, mean fluorescence intensity.

Immediately after stimulation with either S1P or chemokines (CCL19 and CXCL12 elicited similar responses throughout the time course; for simplicity, only CXCL12 is shown), T cells showed prominent membrane ruffling coincident with a burst of actin polymerization (Fig. 7, a and b, Ruffle; and Fig. S3). Both S1P- and chemokine-treated cells then polarized and began actively migrating. During this initial migratory phase (Fig. 7, a and b, Lamellipodial), both sets of cells exhibited broad, flat lamellipodia at the leading edge (arrowheads) and a refractile uropod at the rear. For chemokine-stimulated cells, this morphology was maintained for at least 7 min, when the

assay was terminated. In contrast, S1P-stimulated cells transitioned after 2–3 min from a lamellipodial mode of motility to one associated with prominent membrane blebbing. Blebbing lasted until ~5 min after stimulation, at which point cells characteristically rounded up and ceased migrating (Fig. 7 a, Bleb-based; Video 5; and Video 6). Blebs are sites of temporary PM separation from the actin cortex (Charras and Paluch, 2008; Zatulovskiy et al., 2014). By differential interference contrast (DIC) microscopy, they appear as rapidly forming balloon-like protrusions (Fig. 7 c). Enumeration of these structures revealed that S1P stimulation drove a substantial

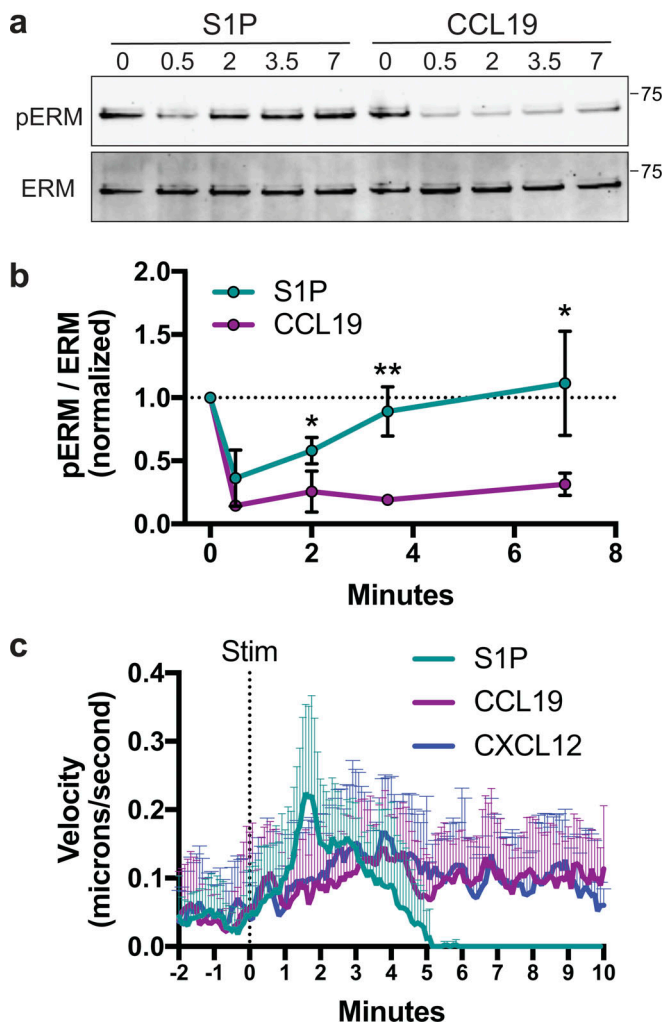


**Figure 5. S1P promotes a rapid, highly transient mode of migration. (a and b)** ERM dephosphorylation and rephosphorylation. WT naive CD4<sup>+</sup> T cells were cultured overnight in media with 10% CS-FBS and then stimulated for 0, 0.5, 2, 3.5, or 7 min with S1P (100 nM) or CCL19 (100 ng/ml), lysed, and immunoblotted for phospho-ERM (pERM; Thr558 for moesin) and total ERM. Quantified band intensities are displayed as the phospho/total ratio. Data are pooled from five independent experiments with means for the S1P and CCL19 group compared at each time point using multiple *t* tests (two-sided) and the Holm-Sidak correction for multiple comparisons. Data distribution was assumed to be normal, but this was not formally tested. Data are displayed as means ± SD, with a dotted line marking the normalized starting value of 1. **(c)** Instantaneous velocity following S1P or chemokine stimulation (Stim). WT naive CD4<sup>+</sup> T cells (previously cultured overnight in media with 10% CS-FBS) were imaged by DIC microscopy before and after stimulation with S1P (100 nM), CCL19 (100 ng/ml), or CXCL12 (100 ng/ml) and manually tracked at 1-s intervals to determine instantaneous velocity. Averages + SD for 12 representative cells per condition are shown. \*, *P* < 0.05; \*\*, *P* < 0.01.

increase in blebbing over unstimulated control cells, whereas chemokine stimulation did not (Fig. 7 d).

Unlike lamellipodia, which are generated when polymerizing actin filaments push against the PM, blebs are powered by intracellular pressure. In resting cells, the PM is tightly associated with the underlying actin cortex, but elevated pressure can force the PM to herniate from cortex, creating a membrane bleb (Charras and Paluch, 2008). To ask if S1P treatment results in

pressurization that could drive bleb-based migration, T cells were left untreated or stimulated with either S1P or CCL19, and intracellular pressure was determined. As shown in Fig. 7 e, S1P stimulation resulted in a significant elevation in intracellular pressure, whereas CCL19 stimulation did not. Since actomyosin contractility is a key regulator of intracellular pressure (Chengappa et al., 2018b), we tested the effects of treating cells with the myosin inhibitor blebbistatin (BBS) before S1P stimulation. Treatment with BBS alone resulted in a significant drop in pressure, consistent with a well-described homeostatic role for myosin contractility in pressure maintenance (Fig. 7 e). Following S1P stimulation, BBS-treated T cells failed to elevate their intracellular pressure (Fig. 7 e), pointing toward a critical role for myosin activity in S1P-induced pressurization.

Many stimuli that induce myosin contractility do so through phosphorylation of myosin light chain (MLC) at Thr18/Ser19, which enhances ATPase activity of the myosin heavy chain head domain (Ikebe et al., 1988; Umemoto et al., 1989; Wendt et al., 2001). We therefore stimulated T cells with S1P or chemokine and assessed MLC phosphorylation by immunoblotting with an antibody that detects phosphorylation at both sites. In S1P-treated cells, MLC phosphorylation rose significantly between 2 and 3.5 min (Fig. 8, a and b), which corresponds temporally with the onset of blebbing observed by video microscopy (Fig. 7 a). Notably, CCL19 did not drive elevation of MLC phosphorylation. Indeed, CCL19 induced a significant decrease in phosphorylation at 0.5 min (Fig. 8, a and b). The failure of CCL19 to induce MLC phosphorylation was not due to a lack of receptor signaling, since both S1P and CCL19 activated the Akt pathway (Fig. 8, a and b). To determine if S1P-induced myosin activation was responsible for blebbing, we repeated the chemokinesis assay in the presence or absence of BBS. As previously detailed in Fig. 7 a, T cells treated with S1P in the absence of inhibitor sequentially ruffle, migrate with lamellipodia, and then migrate with blebs. When myosin was inhibited with BBS, T cells still ruffled in response to S1P. However, most cells subsequently displayed profound polarity defects. In place of the well-defined lamellipodium, these cells formed random pseudopodial protrusions and failed to transition to bleb-based motility, instead rounding up prematurely (Fig. 8 d). Even those BBS-treated cells that polarized normally at early time points subsequently rounded up and failed to bleb properly (Fig. 8 e). Single-cell-tracking analysis revealed that BBS potently inhibited bleb formation and net displacement in S1P-treated T cells (Fig. 8, f and g). Cumulatively, these data indicate that S1P stimulation results in a brief (1–3 min) period of actin polymerization, ruffling, and lamellipodial extension, followed by a period of enhanced myosin contractility, intracellular pressurization, and bleb-based motility.

### ERM proteins facilitate migration by limiting blebs to the leading edge

ERM proteins, which link the PM to the actin cortex, are known to play an important role in bleb prevention and resolution (Charras et al., 2006). We therefore compared bleb formation in WT and DKO T cells during S1P-induced migration. At early times after S1P addition, WT and DKO cells ruffled, polarized,

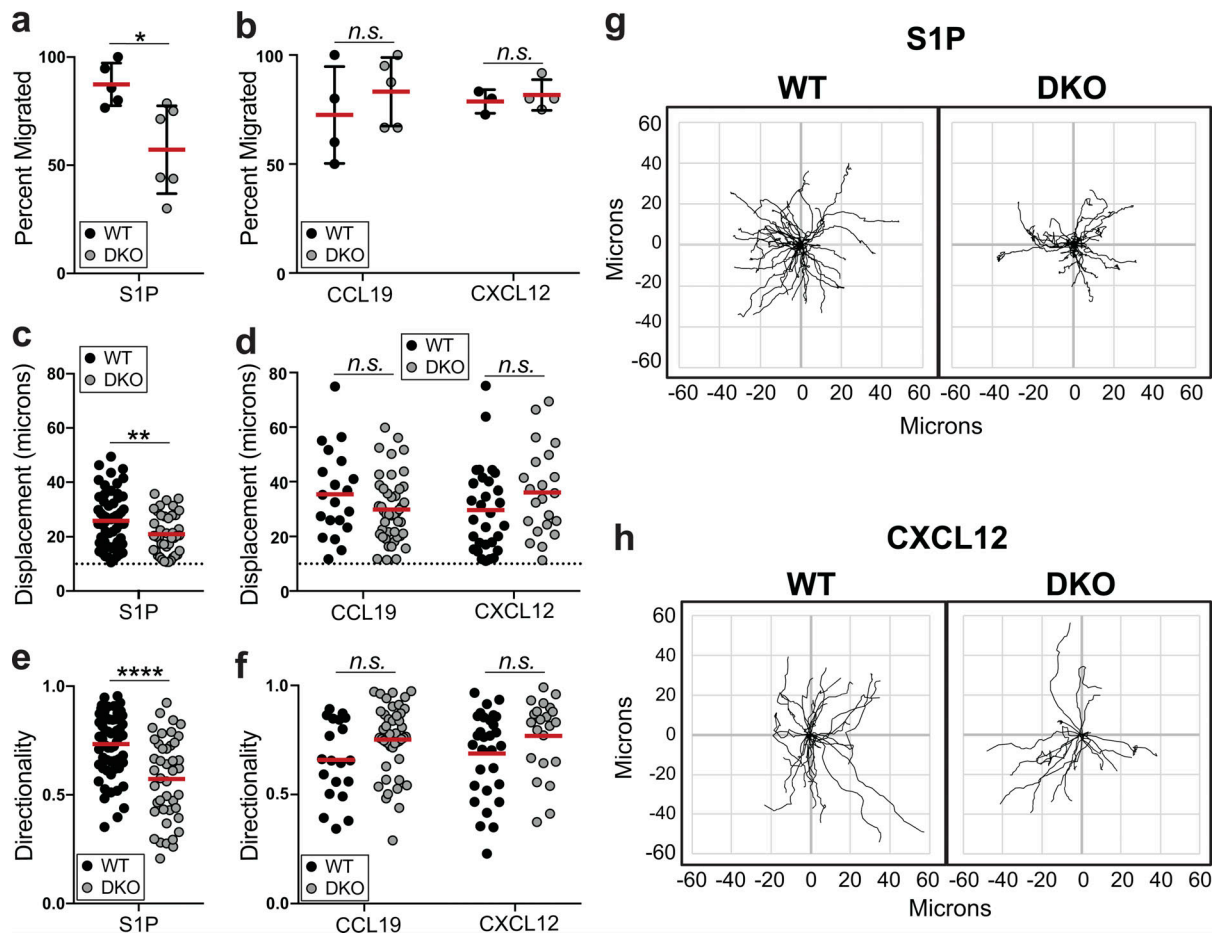


**Figure 6. ERM proteins are required for S1P-induced chemokinetic responses.** (a–h) Cells were cultured overnight in media with 10% CS-FBS, added to VCAM-coated chambers, and monitored by DIC microscopy following stimulation with S1P (100 nM), CCL19 (100 ng/ml), or CXCL12 (100 ng/ml). (a and b) Percentage of cells that displace at least 10  $\mu\text{m}$  during the response. Each dot corresponds to a field of cells pooled from three independent experiments shown. Means  $\pm$  SD are shown and compared individually using *t* tests (two-sided). (c and d) Displacement of WT and DKO migratory cells following S1P or chemokine stimulation. Dashed lines indicate the 10- $\mu\text{m}$  threshold. (e and f) Directionality of migratory WT and DKO cells. Directionality was calculated by dividing displacement by total track length. (c–f) Pooled data from three independent experiments are displayed as individual cells (dots) and means (horizontal bars) and compared using Mann-Whitney (nonparametric) *t* tests. (g and h) Tracks of individual cells with the same origin are shown, representative of three individual experiments. n.s.,  $P > 0.05$ ; \*,  $P < 0.05$ ; \*\*,  $P < 0.01$ ; \*\*\*\*,  $P < 0.0001$ .

and began to migrate similarly (Fig. 9 a). However, when the transition to blebbing occurred, WT T cells displayed blebbing at or near the leading edge, whereas DKO T cells showed indiscriminate blebbing all around the cell body (Fig. 9 a, asterisks; Video 7; and Video 8). To quantify this, cells were divided into thirds along the axis of migration, and the front third was further divided into “front” and “lead” to distinguish blebs that occur strictly at the leading edge. Examples of blebs occurring in each region are shown in Fig. 9 b. Videos of WT and DKO T cells were then analyzed for the bleb frequency within each region. Blebbing in the rear third of the cell was rarely observed in either cell population (Fig. 9 c). In WT T cells, blebbing was progressively more frequent in the regions closer to the leading edge. In contrast, DKO T cells showed blebbing at similar levels across the middle, front, and leading-edge regions. Relative to WT cells, these cells showed elevated blebbing in the middle region and reduced blebbing at the leading edge (Fig. 8 c). In WT cells, bleb area also increased with proximity to the leading

edge, with a particularly sharp increase between the middle and front/lead regions (Fig. 9 d). In contrast, blebs in DKO T cells were large irrespective of location (Fig. 9 d). This inability to spatially regulate bleb frequency and size likely underlies the profound directionality defects displayed by DKO T cells responding to S1P (Fig. 6 e).

Finally, we asked how the location of active ERM proteins within the cell relates to the spatial organization of blebbing. WT T cells bound to VCAM were stimulated with S1P for 1, 2.5, or 5 min, after which they were fixed, labeled for phospho-ERM proteins, and counterstained for tubulin to identify the centrosome, which is positioned in the rear of migratory lymphocytes. Consistent with the Western blot data (Fig. 5, b and c), S1P drove an initial dephosphorylation of ERM proteins that recovered after 2.5–5 min. At 2.5 min, when cells are highly migratory and beginning to bleb, labeling for phosphorylated ERM proteins showed a highly polarized distribution. Label was enriched at the rear of the cell, diminished gradually within the middle



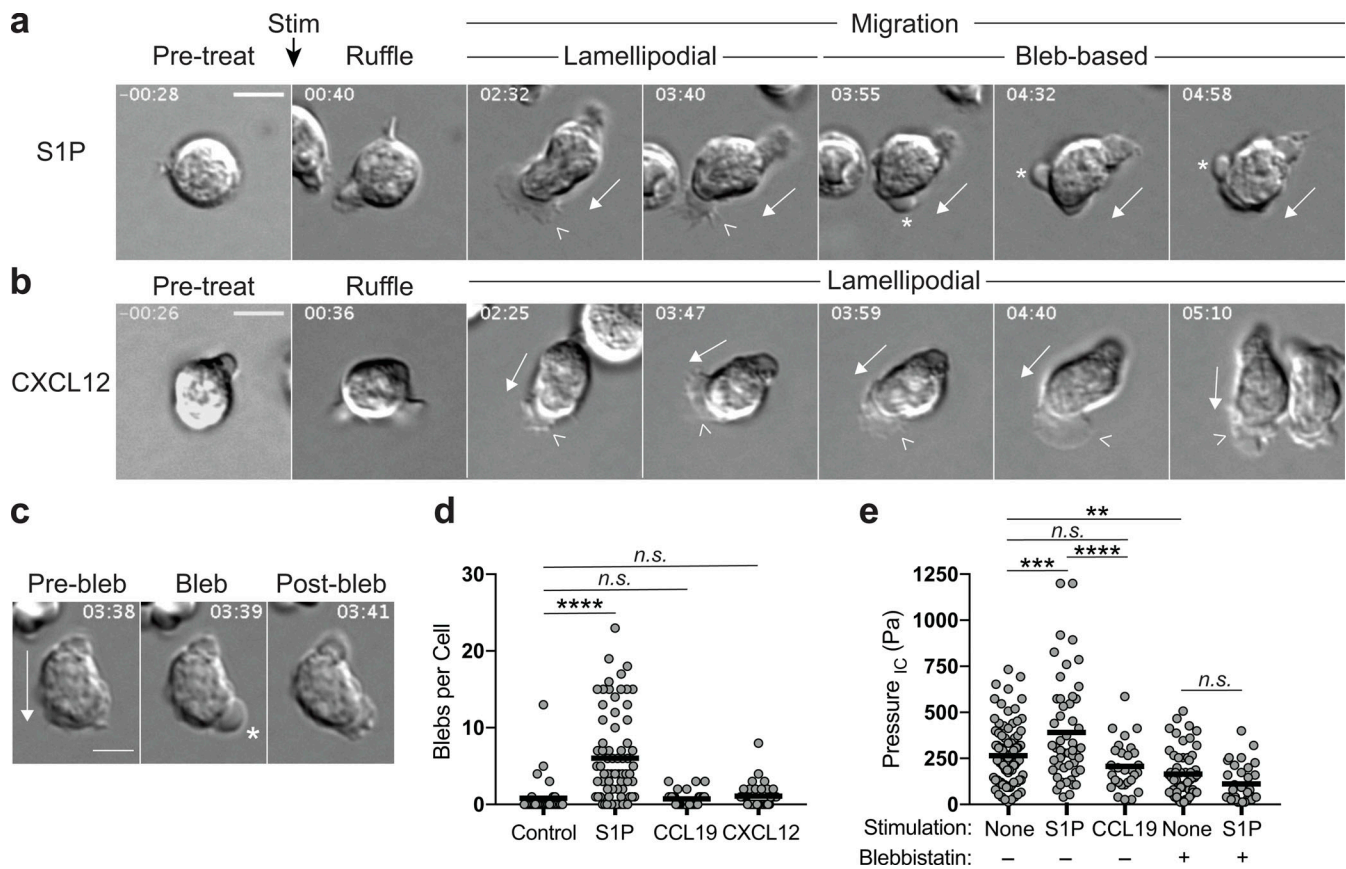


**Figure 7. S1P induces pressurized, bleb-based migration.** (a and b) Representative migratory responses for S1P versus chemokine. WT naive CD4<sup>+</sup> T cells (previously cultured overnight in media with 10% CS-FBS) were imaged by DIC microscopy on VCAM-coated chambers before and after stimulation (Stim) with S1P (100 nM; a), CCL19 (100 ng/ml, not shown), or CXCL12 (100 ng/ml; b). (c) Representative cell showing the rapid formation and transient nature of blebs in migratory cells following S1P treatment. (a–c) Time is in min:s and relative to point of stimulation; scale bars, 5  $\mu$ m. Full arrows indicate direction of migration, arrowheads indicate lamellipodia, and asterisks indicate blebs. (d) Bleb quantitation following S1P or chemokine stimulation as in a. Blebs were manually counted from DIC movies of control, S1P-, or chemokine-stimulated cells on VCAM. Each dot corresponds to a cell pooled from three independent experiments. Means (horizontal bars) of S1P, CCL19, and CXCL12 groups were compared with control using a Kruskal-Wallis (nonparametric) one-way ANOVA. (e) Intracellular pressure following S1P or chemokine stimulation. WT naive CD4<sup>+</sup> T cells (previously cultured overnight in media with 10% CS-FBS) were added to poly-L-lysine-coated plates and left untreated or stimulated with S1P (100 nM) or CCL19 (100 ng/ml). Pressure was measured by the servo null method, collecting readings from as many cells as possible within a 12-min window after stimulation. Where indicated, cells were pretreated with BBS (50  $\mu$ M) for at least 30 min before stimulation. Each dot corresponds to a cell, pooled from four independent experiments. Means (horizontal bars) of all groups compared with each other using a one-way ANOVA with a Tukey correction for multiple comparisons. IC, intracellular; n.s.,  $P > 0.05$ ; \*\*,  $P < 0.01$ ; \*\*\*,  $P < 0.001$ ; \*\*\*\*,  $P < 0.0001$ .

region, and was largely absent from the front third of the cell (Fig. 9, e and f). By 5 min after stimulation, when cells had rounded up and ceased migration, active ERM proteins were found all around the cell cortex. Importantly, the regions where ERM proteins accumulate in WT cells correspond to regions of low bleb frequency. These are the same regions that show elevated bleb frequency and size in DKO T cells. Taken together, these results show that ERM proteins facilitate S1P-induced migration by restricting blebbing to the leading edge.

## Discussion

In this report, we show that S1P promotes a mode of cell motility that is fundamentally different from the response elicited by chemokines. Rather than relying solely on actin polymerization-based lamellipodial migration, S1P promotes pressurization and blebbing, a mode of migration typically reserved for cells

tasked with migrating in confinement (Charras and Paluch, 2008). During this bleb-based migratory response, ERM proteins localize to the rear and sides of polarized T cells, where they tether the PM to the actin cortex. This process restricts blebbing to the leading edge, thereby promoting forward movement of the cell. ERM-deficient T cells show dysregulated blebbing, resulting in compromised chemokinetic and transmigration responses toward S1P in vitro and defective egress from lymphoid tissues in vivo.

The phenotype of our ERM KO mice resembles that of moesin-deficient mice independently derived by Hirata et al. (2012). Our data confirm that moesin deficiency alone causes perturbations in T cell trafficking and extend this by showing that many of these perturbations are worsened by additional loss of ezrin. Our findings indicate that T cell trafficking involves functional overlap between ezrin and moesin, but that moesin (the more abundant isoform) plays a more important role.

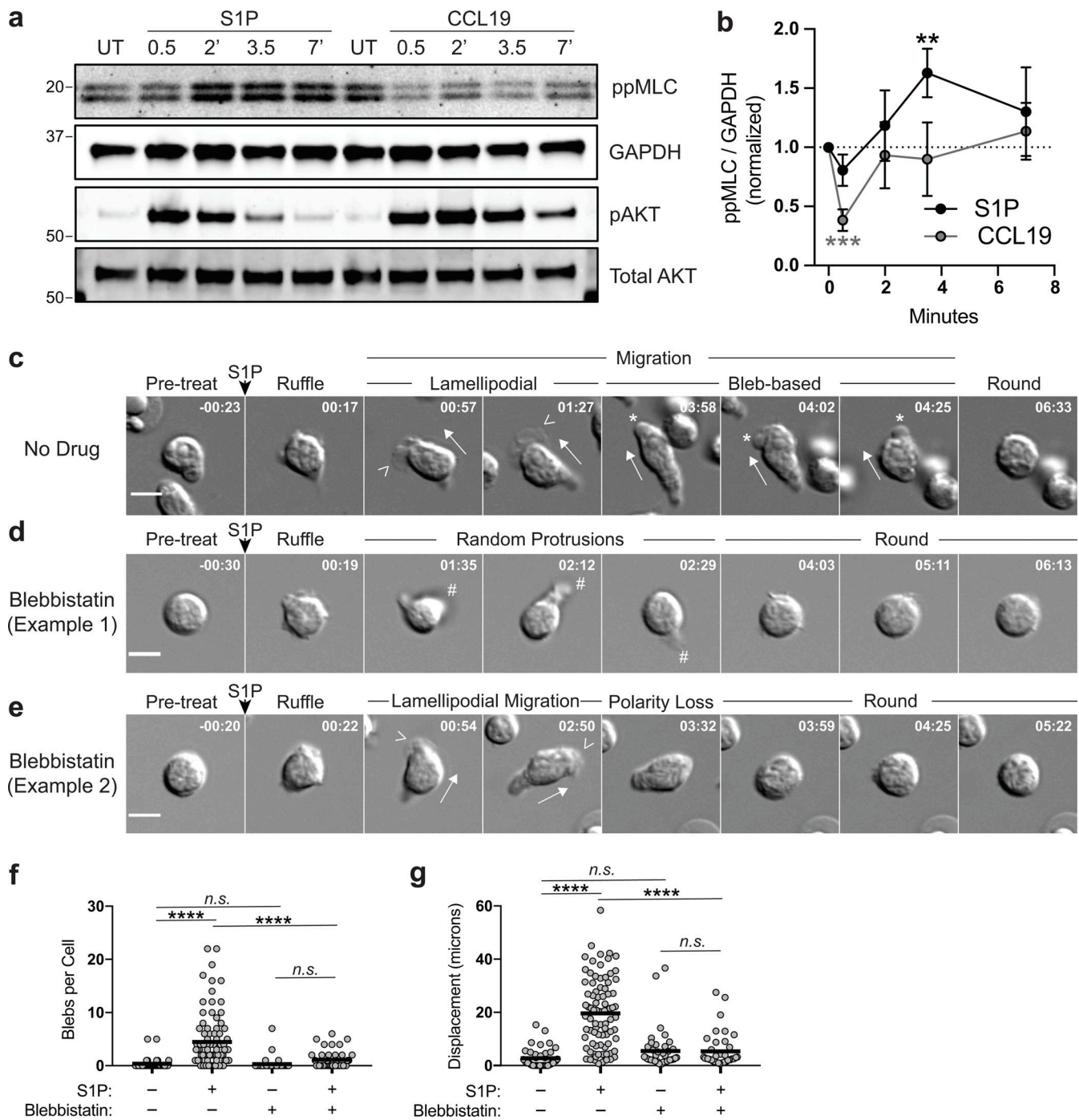


**Figure 8. S1P activates myosin to promote bleb-based motility. (a and b)** WT naive CD4<sup>+</sup> T cells (previously cultured overnight in media with 10% CS-FBS) were stimulated with S1P (100 nM) or CCL19 (100 ng/ml) for the indicated times. Cell lysates were immunoblotted for phospho-MLC (ppMLC; Thr18+Ser19), GAPDH, phospho-AKT (pAKT; Ser473), and total AKT. Band intensities were quantified, and the ratio of ppMLC to GAPDH signal was determined and normalized to 1 for the unstimulated control (indicated with a dotted line). Pooled data from four independent experiments are shown as means  $\pm$  SD (b). For statistical analysis, variation of each experimental sample from the starting value of 1 was tested using a one-sample t test. **(c-e)** WT naive CD4<sup>+</sup> T cells (previously cultured overnight in media with 10% CS-FBS) were imaged by DIC microscopy on VCAM-coated chambers before and after stimulation with S1P (100 nM). Where indicated, cells were pretreated with BBS (5  $\mu$ M) for 10 min. Scale bars, 5  $\mu$ m. Time in min:s and relative to point of stimulation. Full arrows indicate direction of migration, arrowheads indicate lamellipodia, asterisks indicate blebs, and # indicates random pseudopodial protrusions. **(f and g)** Blebs were manually counted, and displacement was tracked from DIC movies. Where indicated, cells were pretreated with BBS (5  $\mu$ M) for 10 min. Each dot corresponds to a cell pooled from two independent experiments. Means (horizontal bars) of groups compared using an ordinary one-way ANOVA with a Tukey correction for multiple comparisons. UT, untreated. \*\*, P < 0.01; \*\*\*, P < 0.001; \*\*\*\*, P < 0.0001.

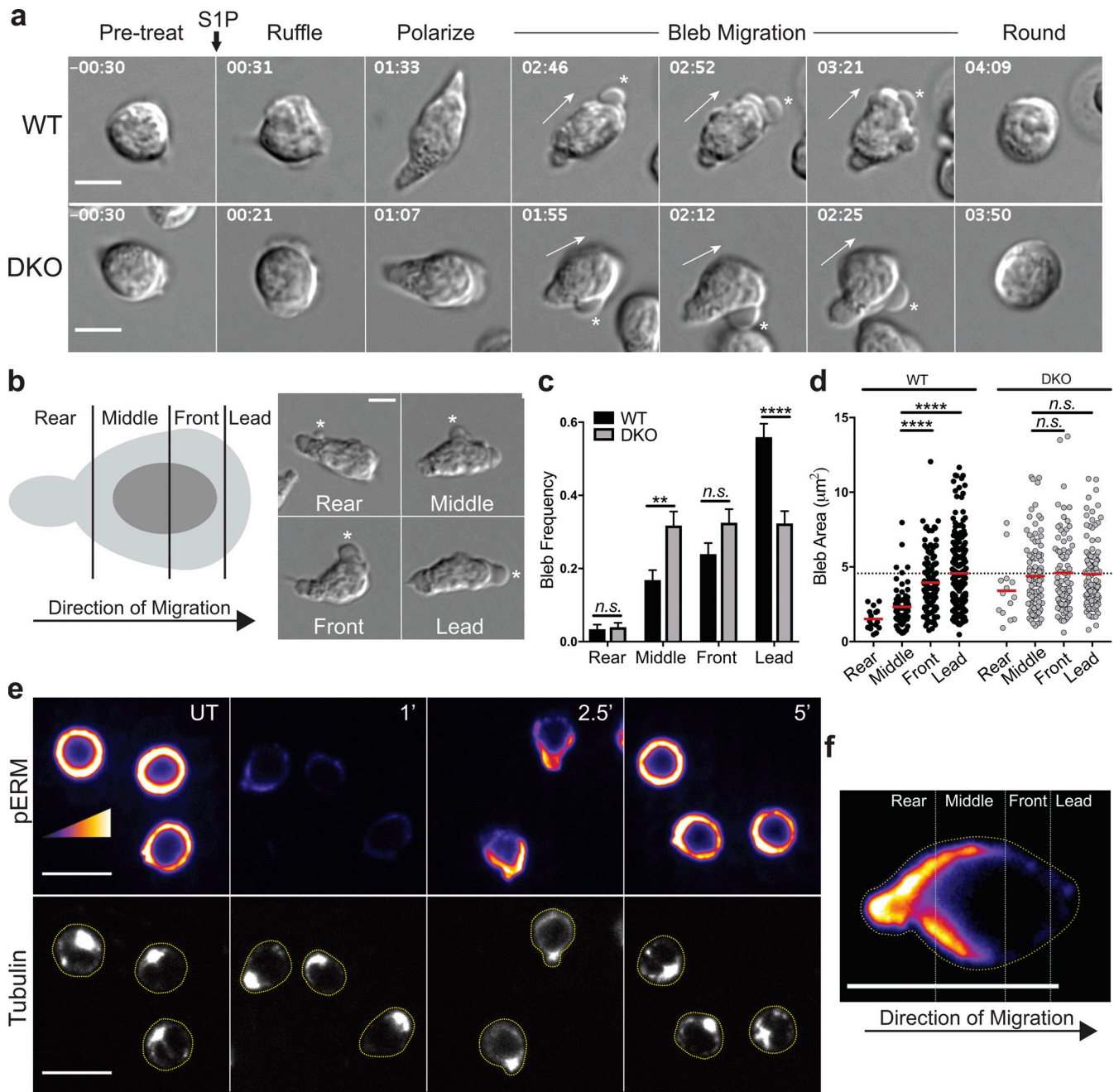


**Figure 9. ERM proteins facilitate S1P-induced migration by limiting blebs to the leading edge.** (a) Representative S1P-induced bleb-based migration for WT and DKO naive CD4<sup>+</sup> T cells. Cells were cultured overnight in media with 10% CS-FBS and imaged by DIC microscopy before and after stimulation with S1P (100 nM). Full arrows indicate direction of migration and asterisks indicate blebs. Time in min:s relative to S1P stimulation. Scale bar, 5 µm. (b) An illustration depicting a cell divided along the axis of migration and an example of S1P-induced blebs occurring in each region (asterisks). (c and d) Bleb frequency and area along the axis of migration. Individual cells were tracked during S1P-induced migration, blebs were binned into the appropriate region, and area was measured. (c) More than 50 cells pooled from three independent experiments shown as the mean ± SEM compared using multiple t tests (two-sided) and the Holm-Sidak correction for multiple comparisons. Data distribution was assumed to be normal, but this was not formally tested. (d) Each dot corresponds to an individual bleb (>300 per group), and means compared (red horizontal bars) using a Kruskal-Wallis (nonparametric) one-way ANOVA. Dashed line at WT lead mean. (e) Active ERM protein localization during S1P migratory responses. WT naive CD4<sup>+</sup> T cells (previously cultured overnight in media with 10% CS-FBS) were stimulated with S1P, fixed at the indicated times after S1P addition (minutes), stained for phospho-ERM proteins (pERM; top) and tubulin (bottom), and imaged by confocal fluorescence microscopy. UT, untreated. Scale bar, 10 µm. Cells are outlined in yellow in the tubulin channel. Representative images from three independent experiments. (f) A representative cell from the 2.5-min time point in e enlarged and oriented in the same direction as in b; scale bar, 10 µm. n.s.,  $P > 0.05$ ; \*\*,  $P < 0.01$ ; \*\*\*\*,  $P < 0.0001$ .

Hirata et al. (2012) also observed an S1P-dependent egress defect in their MKO mice. Using a variety of techniques including splenectomy, integrin blockade, and BrdU labeling, they demonstrated that moesin-deficient T cells display defective egress from the lymph nodes, spleen, and thymus alike.

Hirata et al. (2012) attributed the defective migratory responses they observed to a requirement for moesin in mediating S1P-stimulated actin polymerization. In our hands, S1P-induced actin polymerization was intact in DKO T cells, as were other signaling events downstream of S1PR1. In a subsequent study, the Hirata group reported defects in ligand-induced S1PR1 endocytosis based on qualitative analysis of immunofluorescence images; however, their flow cytometric analysis showed decreased resting surface S1PR1 expression rather than diminished endocytic uptake (Nomachi et al., 2013). In our hands, ERM deficiency had no effect on resting surface S1PR1 levels, consistent with the initial Hirata paper. Moreover, we found no change in the magnitude or kinetics of ligand-driven receptor endocytosis. The basis for these discrepancies is unclear, but one difference is our use of an optimized overnight cell culture protocol, which results in robust responses more suitable for quantitative analysis. Using these optimized conditions, we conclude that ERM proteins are not needed for S1PR1 expression or signaling. Instead, ERM proteins are specifically required for the migratory response elicited by S1P because that response, unlike conventional chemokine responses, utilizes bleb-based motility.

Phosphorylated ERM proteins accumulate at the rear and sides of S1P-stimulated cells, consistent with a model in which polarized blebbing is driven by uniform increases in intracellular pressure and localized weaknesses in the membrane-cortex interaction. This may be the general rule, since cells may not be able to maintain asymmetric intracellular pressure on the time scale needed to drive motility (Strychalski and Guy, 2016; Tinevez et al., 2009). Our findings in T cells are consistent with similar observations in melanoma cells (Lorentzen et al., 2011) and zebrafish primordial germ cells (Diz-Muñoz et al., 2010; Diz-Muñoz et al., 2016). Thus, ERM proteins appear to facilitate bleb-based motility across a variety of cell types and systems. Going forward, it will be interesting to ask if other cortical cytoskeletal proteins also contribute to this process. One candidate group of proteins is the septins, which also constrain blebbing and regulate migratory behavior (Gilden et al., 2012; Tooley et al., 2009).

The stark differences in migratory responses elicited by S1PR1 and CCR7 mirror the differential requirements and function of these receptors in vivo. Homeostatic chemokine receptors like CCR7 promote intranodal migration over relatively large distances and determine the positioning and organization of T cells within lymphoid organs (Braun et al., 2011; Förster et al., 1999; Ohl et al., 2003). For these purposes, a mild but sustained lamellipodial migratory response is well suited. S1PR1, however, does not control migration over large distances, as evidenced by the finding that S1PR1-deficient T cells approach and probe lymphatic sinus egress sites grossly normally (Grigorova et al., 2009). Instead, S1PR1 prompts T cells to cross the porous barrier posed by sinus endothelial cells. Barrier

crossing requires only a few minutes in vivo (Grigorova et al., 2009), matching the duration of the in vitro response elicited by S1P (Fig. 5 c). Similarly, S1P, but not chemokines, promotes T cell transendothelial migration through lymphatic endothelium in vitro (Xiong et al., 2019). We note that the findings reported here are limited to naive T cells and the chemokine receptors they express; differences in cell type and receptor expression may also influence the migratory responses induced by different chemoattractants.

An important question going forward is how T cells use these different modes of motility as they navigate the challenges of in vivo trafficking. Although blebs have been observed in mesenchymal stem cells undergoing transendothelial migration (Teo et al., 2012), blebbing has not been documented for T cells crossing endothelial barriers. Extravasation across blood endothelium has been shown to involve the formation of actin-rich podosomes (Carman et al., 2007); whether blebs also participate is unknown. One interesting possibility is that the mechanism for T cell passage depends on differences in the endothelial barriers themselves. Most blood endothelial cells show continuous expression of adhesion molecules along their junctions to form tight “zipper-like” barriers (Dejana et al., 2009; Shapiro et al., 1995). In contrast, blind-end lymphatic sinus endothelial cells (at least those that drain peripheral tissues) form overlapping flaps with discontinuous adhesion molecules, resulting in “button-like” barriers (Baluk et al., 2007). Passage across zipper-like adhesions requires integrin-mediated motility and actin-rich protrusions (Carman et al., 2007). In contrast, passage across button-like endothelia, which occurs by squeezing through preexisting discontinuities (Pflücke and Sixt, 2009), may be preferentially bleb dependent. This idea is consistent with modeling studies showing that blebs are particularly effective at navigating settings of discontinuous confinement, where they can expand into preexisting discontinuities in the matrix (Tozluoğlu et al., 2013). One obstacle to understanding this aspect of T cell trafficking is the paucity of information about the anatomical nature of many egress portals (Baluk et al., 2007; Jalkanen and Salmi, 2020). S1P-mediated egress from thymus and spleen occurs either primarily or exclusively into blood rather than lymph (Matloubian et al., 2004; Pappu et al., 2007; Zachariah and Cyster, 2010), but it is unclear if these vascular egress portals resemble typical zipper-like blood endothelium or button-like lymphatic sinuses. Egress portals in the spleen have remained ill-defined despite extensive efforts (Chauveau et al., 2020), and egress portals in the thymus possess notable anatomical differences from standard blood endothelium, including a prominent perivascular space (Mori et al., 2007; Zachariah and Cyster, 2010). We propose that the protrusive mechanism used by an egressing T cell likely will depend upon the type of barrier encountered, but further studies using in vivo imaging approaches are needed.

Using direct intracellular pressure measurements, we demonstrate that T cells undergo pressurization following stimulation with S1P but not CCL19. To our knowledge, this is the first time that intracellular pressure has been directly measured in any leukocyte subset. We find that T cells maintain a slightly lower intracellular pressure than other mammalian cells

measured by the same method (Chengappa et al., 2018a; Petrie and Koo, 2014). Our data indicate that increased myosin contractility drives increased intracellular pressure in SIP-treated cells. In keeping with this, myosin-deficient T cells display prolonged lymph node retention, consistent with an egress defect (Jacobelli et al., 2010). Interestingly, both myosin-deficient and ERM-deficient T cells exhibit defective chemotaxis toward conventional chemokines when asked to pass through 3- $\mu$ m pores, but not the 5- $\mu$ m pores used in this study (Chen et al., 2013; Jacobelli et al., 2013). Similarly, myosin becomes increasingly important for integrin-independent dendritic cell migration as the extracellular matrix becomes more restrictive (Chabaud et al., 2015; Lämmermann et al., 2008). Thus, it appears that myosin promotes cell motility in different ways depending on chemical and physical cues. In confined spaces, myosin propels cells forward, whereas in T cells responding to SIP, myosin powers pressurized bleb-based migration even in the absence of confinement.

Although our studies point to a clear role for myosin, regulated solute transport could also influence intracellular pressure (Chengappa et al., 2018a). Aquaporins can coordinate migration in some settings by harnessing osmotic pressure (Stroka et al., 2014), and treating mice with a putative inhibitor of aquaporin 4 results in potent lymphopenia without changes in splenic T cell numbers, consistent with an egress block. These alterations were attributed to changes in gene expression, but a direct role for aquaporins in egress was not ruled out (Nicosia et al., 2019). In our hands, T cells poorly tolerated inhibitors of aquaporins and solute transporters, precluding studies aimed at determining a role for osmolarity in SIP-induced pressurization or blebbing.

Our work reveals that lymphocyte trafficking involves a previously unrecognized level of plasticity, with different chemical cues eliciting specialized motile strategies depending on tissue context. Going forward, it will be important to define the in vivo contexts where bleb-based motility is important, and to ask how cells integrate distinct motile responses as they respond to competing environmental cues.

## Materials and methods

### Mice

MKO mice were generated by and purchased from the Texas A&M Institute for Genomic Medicine. A gene trap vector was inserted into the first intron of the *Msn* gene on the X chromosome in 129/Sv ES clones (OST432827), and live mice with germline insertion were generated on the 129Sv  $\times$  C57BL/6 background. The resulting MKO mice were backcrossed for 10 generations to mice of the C57BL/6 background (The Jackson Laboratory). Mice homozygous for a floxed ezrin gene and transgenic for CD4-Cre on the C57BL/6 background (EKO; Shaffer et al., 2009) were then crossed to the MKO mice to generate mice bearing germline deletion of moesin and deletion of ezrin late in T cell development (female: *Msn*<sup>-/-</sup> *Ezrin*<sup>flox/flox</sup>CD4-Cre<sup>+</sup> or male: *Msn*<sup>-/Y</sup> *Ezrin*<sup>flox/flox</sup>CD4-Cre<sup>+</sup>). For most experiments, sex-matched WT littermates were used as controls. Age- and sex-matched controls were used when littermates were not available or

possible. All mice were housed under barrier conditions in the Children's Hospital of Philadelphia animal facility, in accordance with protocols approved by the Institutional Animal Care and Use Committee.

### Flow cytometry

Spleens, lymph nodes, and thymi were harvested from 8–16-wk-old mice, and single-cell suspensions were prepared. Peripheral blood mononuclear cells were isolated with Lymphoprep (STEMCELL). Cells were counted and stained with the following fluorochrome-conjugated antibodies: FITC anti-CD3 (Biolegend; Cat. #100204), BV786 anti-CD4 (BD Biosciences; Cat. #56331), FITC anti-CD4 (Biolegend; Cat. #116004), APC anti-CD4 (Biolegend; Cat. #100516), PE anti-CD4 (Biolegend; Cat. #100512), APC anti-CD8 (Biolegend; Cat. #100712), PE/Cy7 anti-CD8 (Biolegend; Cat. #100722), BV605 anti-CD44 (BD Biosciences; Cat. #563058), PE anti-CD62L (Biolegend; Cat. #104407), PerCP/Cy5.5 anti-NK1.1 (Biolegend; Cat. #108727), and live-dead aqua or blue (Thermo Fisher Scientific; Cat. #L34957 and #L23105). For SIPRI, staining was done in lipid-free FACS buffer (PBS + 1% CS-FBS + 1 mM EDTA). Cells were stained sequentially with rat anti-SIPRI (R&D; Cat. #MAB7089), donkey anti-rat IgG-biotin F(ab')<sub>2</sub> (Jackson ImmunoResearch; Cat. #712-066-153), and Streptavidin-APC (Biolegend; Cat. #405207). For SIPRI endocytosis experiments, cells were stimulated with SIP (10 nM) for the indicated times, and endocytosis was stopped by adding ice-cold PBS and washing twice with lipid-free FACS buffer before surface staining. For F-actin measurements, cells were stimulated with SIP (1 nM) or CCL19 (100 ng/ml) and fixed with 3% PFA at the indicated times. Cells were then permeabilized with PSG (PBS + 0.01% saponin + 0.25% fish skin gelatin) and labeled with phalloidin AlexaFluor 488 (Invitrogen) and rat anti-CD4-APC (Clone RM4-5, BioLegend; Cat. #100506). All samples were analyzed on either an LSR Fortessa or LSRII (BD Biosciences) equipped with FACSDiva software (BD Biosciences). Data were analyzed using FlowJo software (v.10.4.2). Representative gating strategies for all experiments involving flow cytometry are shown in Fig. S4.

### Immunofluorescence microscopy on tissue sections

Spleens and lymph nodes were fixed for 2–4 h in 4% PFA in PBS, washed, and incubated overnight in 30% sucrose in PBS. Tissues were embedded in OCT and sectioned using a cryostat. Sections were blocked for 30 min in staining solution (5% donkey serum in PBS-Tween) containing FcRblock and subsequently incubated overnight at 4°C in staining solution with 1–2 ng/ $\mu$ l anti-CD3-AlexaFluor 647 (Clone 17A2, Biolegend; Cat. #100209), anti-B220-Brilliant Violet 421 (Clone RA3-6B2, Biolegend; Cat. #103239), and rabbit anti-laminin 1+2 (Abcam; Cat. #AB7463) labeled with CF568 Mix-n-stain kit (Biotium). After washing in PBS, slides were mounted using ProLong Diamond antifade (Invitrogen) and imaged at room temperature using a Zeiss LSM710 AxioObserver inverted confocal microscope. Images were captured using Zen 2012 (Zeiss) software and analyzed with Volocity v6.3 (Perkin Elmer) software with  $\gamma = 1.00$ .

### Competitive in vivo migration

Naive CD4<sup>+</sup> T cells isolated from the spleens and lymph nodes of age- and sex-matched DKO (CD45.2<sup>+</sup>) and congenic WT CD45.1<sup>+</sup> B6.SJL-Ptprc<sup>a</sup> mice (The Jackson Laboratory) were labeled with 1  $\mu$ M CellTracker Green CMFDA (Thermo Fisher Scientific), washed, and mixed at a 1:1 ratio in PBS. 10<sup>6</sup> total cells were injected into the tail veins of recipient animals. Recipients were euthanized at 1 or 24 h after injection. Cells from blood, spleens, and lymph nodes were harvested, stained with BUV395 anti-CD4 (BD Biosciences; Cat. #563790), V450 anti-CD45.1 (Tonbo; Cat. #75-04530-U025), APC anti-CD45.2 (Tonbo; Cat. #20-0454-U025), and Ghost Dye Red 780 Live/Dead stain (Tonbo; Cat. #13-0865-T100) and analyzed by flow cytometry. Input cells were analyzed in parallel. CellTracker Green was used to distinguish between donor and recipient cells, and WT and DKO were further distinguished by CD45.1/CD45.2 expression. Final ratios were normalized to the corresponding input ratios.

### T cell purification and culture

For functional studies, lymphoid organs were harvested into ice-cold PBS, 0.5% fatty acid-free BSA, and 1 mM EDTA (MACS Buffer), and cell suspensions were prepared. Naive CD4<sup>+</sup> T cells were harvested by negative magnetic selection (Miltenyi), washed extensively in MACS buffer, and resuspended in DMEM with 10% CS-FBS (Gibco). Cells were cultured overnight at 37°C and 10% CO<sub>2</sub> before use.

### S1P preparation

S1P d18:1 (Avanti) powder was solubilized in methanol:water 95:5 at 50°C with sonication. The solvent was evaporated using dry nitrogen to create a film of S1P on the interior of the vessel, which was resuspended in Milli-Q water supplemented with 4 mg/ml of fatty acid-free BSA (Roche) to a final concentration of 100  $\mu$ M. The S1P-BSA solution was stored at -20°C in tightly sealed glass vials and diluted into cell culture media immediately before use.

### Transwell assays

10<sup>5</sup> T cells in DMEM supplemented with 10% CS-FBS were added into a 5- $\mu$ m transwell insert (Corning) and allowed to settle for 20 min. The insert was gently lowered into a well containing the indicated chemoattractant. In some experiments, the 20-min settling phase doubled as a preincubation with 100 nM of Ex26 (Tocris). An identical concentration of the drug was included in the lower chamber. After 90 min, transwell inserts were gently removed, and the cells in the lower chamber were enumerated on a hemocytometer.

### Microscopy

For live cell imaging, eight-well chambers (Lab-Tek; Cat. #1.0 Borosilicate) were coated with 2  $\mu$ g/ml recombinant mouse VCAM-1 (R&D) overnight at 4°C and washed before use. Cells were resuspended in Phenol Red-free L-15 medium (Gibco) + glucose (2 mg/ml), allowed to settle in the chambers for 30 min, and then imaged by DIC microscopy at 37°C using either a 40 $\times$  Plan Neofluar (1.3 NA) or a 63 $\times$  Planapo (1.4 NA) objective on a Zeiss Axiovert 200M microscope and an ORCA-ER CCD camera

(Hamamatsu). Time-lapse images were acquired using Slide-book 6 software (Intelligent Imaging Innovations Inc.). Cells were imaged for several minutes at which point S1P, CCL19, or CXCL12 was dripped into the chamber, and acquisition was continued for 10 min. Where indicated, cells were pretreated with 5  $\mu$ M s-nitro-BBS (Tocris) for 10 min before stimulation. Images were collected at 1-s intervals. For immunofluorescence microscopy of fixed cells, cells were allowed to adhere to VCAM-coated surfaces and stimulated with S1P as described above for live cell imaging. At the indicated time after addition of S1P, the medium was gently removed, and the cells were fixed for 20 min in a solution of 10% wt/vol trichloroacetic acid to preserve ERM phosphorylation (Hayashi et al., 1999). Cells were then permeabilized with 0.1% Triton X-100 in PBS, blocked with PBS, 0.01% saponin, and 0.25% gelatin (PSG), stained with rabbit anti-phospho ERM (Cell Signaling; Cat. #141) and rat anti-tubulin (clone YL1/2, Millipore/Sigma; Cat. #MAB1864-1) for 1 h in PSG, washed three times, stained with anti-rabbit Alexa-Fluor 647 and anti-rat AlexaFluor 488 (Invitrogen), washed, covered in PBS, and imaged using a 63 $\times$  1.4 NA Planapo objective on an Axiovert 200M (Zeiss) with a spinning disk confocal system (UltraVIEW ERS6; Perkin Elmer) equipped with an ORCA-Flash 4.0 CMOS camera (Hamamatsu). Images were acquired using Volocity v6.3 software (Perkin Elmer) and were prepared for publication using ImageJ (National Institutes of Health). Contrast and brightness were adjusted using the same settings for all images within an experiment, with  $\gamma = 1.00$ .

### Cell tracking

DIC chemokinesis assay movies were exported into ImageJ, and cells were tracked using the Manual Tracking plugin. To analyze velocity (Fig. 5 c), 12 representative cells were tracked at the 1-s acquisition rate, and the instantaneous velocity was smoothed over 5-s intervals before displaying. For ease, most videos were reduced to every fifth frame before tracking. The different response kinetics with S1P and chemokines forced us to analyze and track cells in each stimulation condition differently. Following stimulation, S1P-treated cells were tracked until the cell characteristically stopped migrating and rounded up, which generally occurred 4–5 min after stimulation (Fig. 5 c). Given the slower but more sustained chemokine response, chemokine-treated cells were tracked for 7 min. Due to these differences in analysis, the different treatment conditions are graphed separately. Cells that left the field of view, landed after stimulation, or dislodged while tracking were not included. Dislodgement was a minor issue for S1P-treated cells and generally only occurred after the cell had rounded up. Dislodgement was a serious issue with CCL19 and CXCL12 treatment, affecting roughly half of the otherwise analyzable cells. We considered this a tolerable problem since it allowed S1P and chemokine treatments to be compared under the same experimental conditions.

### Bleb quantitation

In order for a protrusion to be classified as a bleb by DIC microscopy, three criteria had to be met. First, the protrusion had to form rapidly, generally in <1 s. Second, the edge of the bleb

had to appear smooth and symmetrical, which contrasts with the roughness and irregularity of actin-rich protrusions and edges. Third, the contents of the protrusion had to be clear and devoid of any obvious granules or organelles. These metrics were modified from [Zatulovskiy et al. \(2014\)](#). Once a bleb was identified, it was outlined in ImageJ, and the area was calculated. Based on the direction of migration, the bleb was then determined to have occurred in either the rear, middle, front, or lead regions of the cell.

### Western blotting

For experiments involving stimulation, 200  $\mu$ l of cells in DMEM was added to an Eppendorf tube and stimulated with 50  $\mu$ l of 5 $\times$  S1P (1 nM final). To stop, 1 ml of ice-cold PBS was added, and cells were rapidly centrifuged and resuspended in lysis buffer (50 mM Tris-HCl, 50 mM NaCl, 5 mM EDTA, 50 mM NaF, 30 mM Na<sub>4</sub>P<sub>2</sub>O<sub>7</sub>, 50 mM  $\beta$ -glycerophosphate, and 1% Triton X-100 in water). Cells were lysed on ice for 30 min with occasional vortexing, then microfuged for 10 min. For Western blots aimed at probing for phospho-MLC or phospho-ERM, cell pellets were instead resuspended in 95°C lysis buffer (50 mM Tris-HCl, 300 mM NaCl, 1 mM EDTA, 50 mM NaF, 30 mM Na<sub>4</sub>P<sub>2</sub>O<sub>7</sub>, and 1% SDS in water). Both lysis buffers contained EDTA-free protease inhibitor cocktails (Roche). Irrespective of lysis method, lysates were moved to tubes containing NuPAGE LDS sample buffer (Thermo Fisher Scientific) and boiled for 5 min. Samples were then resolved on Bis-Tris 4–12% gradient or 10% gels (NuPAGE), transferred to nitrocellulose membranes, washed with TRIS-buffered saline with 0.1% TWEEN 20 detergent (TBST), and immunoblotted overnight at 4°C in 2% BSA (wt/vol) TBST. The following antibodies were used for immunoblotting in this report: rabbit anti-ERM (Cell Signaling Technology; Cat. #3142), mouse anti-moesin (clone 38, BD Biosciences; recognizes all family members), rabbit anti-phospho ERM (Cell Signaling; Cat. #3141), mouse anti-GAPDH (Clone 6C5, Millipore Sigma; Cat. #MAB374), rabbit anti-GAPDH (Cell Signaling; Cat. #2118), rabbit anti-phospho Erk1/2 Thr202/Tyr204 (Cell Signaling; Cat. #9101), rabbit anti-phospho Akt Ser473 (Cell Signaling; Cat. #4060), mouse anti-total AKT (Cell Signaling; Cat. #2920), and rabbit anti-phospho-MLC Thr18/Ser19 (Cell Signaling; Cat. #3674). Following overnight incubation, membranes were washed multiple times with TBST and then stained with anti-rabbit or anti-mouse secondary antibodies conjugated to Alexa-Fluor680 (Thermo Fisher Scientific) or IRDye 800CW (Licor). Immunoblots were read on a Licor Odyssey imaging system and quantified using ImageStudioLite (v. 5.2.5, Licor), taking care to remain within the linear range. The positions of molecular weight standards (Biorad; 1610374) are indicated on each blot in kilodaltons.

### Measuring intracellular pressure

The intracellular pressure of T cells was directly measured using the micropressure measurement technique ([Petrie and Koo, 2014](#)). We used a 900A micropressure system (World Precision Instruments) connected to a 0.5- $\mu$ M micropipette filled with 1 M KCl and calibrated in a chamber with 0.1 M KCl solution to set the overall electrical resistance of the system to zero

(null). When measuring intracellular pressure, the tip of the micropipette is inserted through the PM. A positive intracellular pressure pushes the electrolyte solution up the micropipette, and the micropressure machine compensates by increasing the pressure of an air column until a null setting is restored, yielding a pressure value equivalent to the intracellular pressure. An MPC-325 micromanipulator (Sutter Instrument) installed on an LSM700 laser scanning confocal microscope (Zeiss) was used to position the micropipette within the chamber maintained at 37°C and 10% CO<sub>2</sub>. For these experiments, T cells (previously cultured overnight in media with 10% CS-FBS) were plated in chambers coated with poly-L-lysine (Sigma) in DMEM. Cells were left untreated (control) or stimulated with either S1P or CCL19. After each cell was penetrated, pressure measurements were taken for 2–3 s, and the average pressure reading during this interval was taken as the cytoplasmic hydraulic pressure of the cell. Readings were collected from as many cells as possible within a 12-min window after stimulation before moving to a new plate. Where indicated, cells were pretreated with 50  $\mu$ M BBS (Thermo Fisher Scientific) for at least 20 min before stimulation.

### Statistical analysis

All statistical tests were performed and graphs were made using GraphPad Prism (GraphPad Software v7.0d), with specific tests indicated in figure legends. P values were denoted on graphs as follows: n.s., P > 0.05; \*, P < 0.05; \*\*, P < 0.01; \*\*\*, P < 0.001; \*\*\*\*, P < 0.0001.

### Online supplemental material

[Fig. S1](#) shows a schematic of the *Msn* targeting strategy. [Fig. S2](#) shows spleen weights and histological analysis of secondary lymphoid organs in DKO mice. [Fig. S3](#) shows flow cytometric analysis of actin polymerization kinetics in T cells stimulated with S1P or chemokine. [Fig. S4](#) shows gating strategies used for flow cytometry. [Video 1](#) shows WT T cells undergoing S1P-induced chemokinesis. [Video 2](#) shows WT T cells undergoing CCL19-induced chemokinesis. [Video 3](#) shows WT T cells undergoing CXCL12-induced chemokinesis. [Video 4](#) shows DKO T cells undergoing S1P-induced chemokinesis. [Video 5](#) and [Video 6](#) show two examples of the lamellipodia-to-bleb transition induced by S1P. [Video 7](#) and [Video 8](#) show DKO T cell blebbing, with the cell shown in [Video 7](#) exemplifying poor displacement and the cell shown in [Video 8](#) exemplifying poor directionality.

### Acknowledgments

We thank Drs. C. Liu and T. Baumgart for help with S1P preparation, Dr. S. Li for genotyping, A. Allman and the Cell and Developmental Biology Microscopy Core for their help with tissue sectioning and imaging, and members of the Burkhardt laboratory for helpful discussions and critical reading of the manuscript.

This work was supported by National Institutes of Health grants R01 HL128551 to J.K. Burkhardt, R01 AI 091627 to I. Maillard, and R01 GM126054 to R.J. Petrie. T.F. Robertson was supported by T32 HD083185.

The authors declare no competing financial interests.

Author contributions: T.F. Robertson designed and executed most experiments, interpreted the data, and wrote the manuscript. D. Gomez Atria and I. Maillard designed and performed the immunofluorescence imaging studies, and P. Chengappa and R.J. Petrie designed and performed the intracellular pressure experiments. C.F. Wu assisted with T cell purification and culture and transwell migration assays. L. Avery helped design and execute competitive in vivo migration experiments, and N.H. Roy provided conceptual and technical assistance with cell motility and blebbing. J.K. Burkhardt oversaw the project and wrote the manuscript.

Submitted: 28 July 2020

Revised: 7 February 2021

Accepted: 3 March 2021

## References

- Allende, M.L., J.L. Dreier, S. Mandala, and R.L. Proia. 2004. Expression of the sphingosine 1-phosphate receptor, S1P1, on T-cells controls thymic emigration. *J. Biol. Chem.* 279:15396–15401. <https://doi.org/10.1074/jbc.M314291200>
- Arnon, T.I., Y. Xu, C. Lo, T. Pham, J. An, S. Coughlin, G.W. Dorn, and J.G. Cyster. 2011. GRK2-dependent S1PR1 desensitization is required for lymphocytes to overcome their attraction to blood. *Science*. 333: 1898–1903. <https://doi.org/10.1126/science.1208248>
- Bai, Z., H. Hayasaka, M. Kobayashi, W. Li, Z. Guo, M.H. Jang, A. Kondo, B.I. Choi, Y. Iwakura, and M. Miyasaka. 2009. CXC chemokine ligand 12 promotes CCR7-dependent naive T cell trafficking to lymph nodes and Peyer's patches. *J. Immunol.* 182:1287–1295. <https://doi.org/10.4049/jimmunol.182.3.1287>
- Baluk, P., J. Fuxe, H. Hashizume, T. Romano, E. Lashnits, S. Butz, D. Vestweber, M. Corada, C. Molendini, E. Dejana, and D.M. McDonald. 2007. Functionally specialized junctions between endothelial cells of lymphatic vessels. *J. Exp. Med.* 204:2349–2362. <https://doi.org/10.1084/jem.20062596>
- Braun, A., T. Worbs, G.L. Moschovakis, S. Halle, K. Hoffmann, J. Bölter, A. Münk, and R. Förster. 2011. Afferent lymph-derived T cells and DCs use different chemokine receptor CCR7-dependent routes for entry into the lymph node and intranodal migration. *Nat. Immunol.* 12:879–887. <https://doi.org/10.1038/ni.2085>
- Brown, M.J., R. Nijhara, J.A. Hallam, M. Gignac, K.M. Yamada, S.L. Erlandsen, J. Delon, M. Kruhlak, and S. Shaw. 2003. Chemokine stimulation of human peripheral blood T lymphocytes induces rapid dephosphorylation of ERM proteins, which facilitates loss of microvilli and polarization. *Blood*. 102:3890–3899. <https://doi.org/10.1182/blood-2002-12-3807>
- Cahalan, S.M., P.J. Gonzalez-Cabrera, N. Nguyen, M. Guerrero, E.A.G. Cisar, N.B. Leaf, S.J. Brown, E. Roberts, and H. Rosen. 2013. Sphingosine 1-phosphate receptor 1 (S1P1) upregulation and amelioration of experimental autoimmune encephalomyelitis by an S1P1 antagonist. *Mol. Pharmacol.* 83:316–321. <https://doi.org/10.1124/mol.112.082958>
- Carman, C.V., P.T. Sage, T.E. Sciuto, M.A. de la Fuente, R.S. Geha, H.D. Ochs, H.F. Dvorak, A.M. Dvorak, and T.A. Springer. 2007. Transcellular diapedesis is initiated by invasive podosomes. *Immunity*. 26:784–797. <https://doi.org/10.1016/j.immuni.2007.04.015>
- Chabaud, M., M.L. Heuzé, M. Bretou, P. Vargas, P. Maiuri, P. Solanes, M. Maurin, E. Terriac, M. Le Berre, D. Lankar, et al. 2015. Cell migration and antigen capture are antagonistic processes coupled by myosin II in dendritic cells. *Nat. Commun.* 6:7526. <https://doi.org/10.1038/ncomms8526>
- Charras, G., and E. Paluch. 2008. Blebs lead the way: how to migrate without lamellipodia. *Nat. Rev. Mol. Cell Biol.* 9:730–736. <https://doi.org/10.1038/nrm2453>
- Charras, G.T., C.-K. Hu, M. Coughlin, and T.J. Mitchison. 2006. Reassembly of contractile actin cortex in cell blebs. *J. Cell Biol.* 175:477–490. <https://doi.org/10.1083/jcb.200602085>
- Chauveau, A., G. Pirgova, H.W. Cheng, A. De Martin, F.Y. Zhou, S. Wideman, J. Rittscher, B. Ludewig, and T.I. Arnon. 2020. Visualization of T Cell Migration in the Spleen Reveals a Network of Perivascular Pathways that Guide Entry into T Zones. *Immunity*. 52:794–807.e7. <https://doi.org/10.1016/j.immuni.2020.03.010>
- Chen, E.J.H., M.H. Shaffer, E.K. Williamson, Y. Huang, and J.K. Burkhardt. 2013. Ezrin and moesin are required for efficient T cell adhesion and homing to lymphoid organs. *PLoS One*. 8:e52368. <https://doi.org/10.1371/journal.pone.0052368>
- Chengappa, P., K. Sao, T.M. Jones, and R.J. Petrie. 2018a. Chapter seven - Intracellular pressure: A driver of cell morphology and movement. *In International Review of Cell and Molecular Biology*. Vol. 337. L. Galuzzi, editor. Academic Press, Cambridge, MA. 185–211.
- Chengappa, P., K. Sao, T.M. Jones, and R.J. Petrie. 2018b. Intracellular Pressure: A Driver of Cell Morphology and Movement. *Int. Rev. Cell Mol. Biol.* 337:185–211. <https://doi.org/10.1016/bs.ircmb.2017.12.005>
- Cyster, J.G., and S.R. Schwab. 2012. Sphingosine-1-phosphate and lymphocyte egress from lymphoid organs. *Annu. Rev. Immunol.* 30:69–94. <https://doi.org/10.1146/annurev-immunol-020711-075011>
- Dejana, E., F. Orsenigo, C. Molendini, P. Baluk, and D.M. McDonald. 2009. Organization and signaling of endothelial cell-to-cell junctions in various regions of the blood and lymphatic vascular trees. *Cell Tissue Res.* 335:17–25. <https://doi.org/10.1007/s00441-008-0694-5>
- Diz-Muñoz, A., M. Krieg, M. Bergert, I. Ibarlucea-Benitez, D.J. Muller, E. Paluch, and C.-P. Heisenberg. 2010. Control of directed cell migration in vivo by membrane-to-cortex attachment. *PLoS Biol.* 8:e1000544. <https://doi.org/10.1371/journal.pbio.1000544>
- Diz-Muñoz, A., P. Romanczuk, W. Yu, M. Bergert, K. Ivanovitch, G. Salbreux, C.-P. Heisenberg, and E.K. Paluch. 2016. Steering cell migration by alternating blebs and actin-rich protrusions. *BMC Biol.* 14:74. <https://doi.org/10.1186/s12915-016-0294-x>
- Fehon, R.G., A.I. McClatchey, and A. Bretscher. 2010. Organizing the cell cortex: the role of ERM proteins. *Nat. Rev. Mol. Cell Biol.* 11:276–287. <https://doi.org/10.1038/nrm2866>
- Fieviet, B.T., A. Gautreau, C. Roy, L. Del Maestro, P. Mangeat, D. Louvard, and M. Arpin. 2004. Phosphoinositide binding and phosphorylation act sequentially in the activation mechanism of ezrin. *J. Cell Biol.* 164: 653–659. <https://doi.org/10.1083/jcb.200307032>
- Förster, R., A. Schubel, D. Breitfeld, E. Kremmer, I. Renner-Müller, E. Wolf, and M. Lipp. 1999. CCR7 coordinates the primary immune response by establishing functional microenvironments in secondary lymphoid organs. *Cell*. 99:23–33. [https://doi.org/10.1016/S0092-8674\(00\)80059-8](https://doi.org/10.1016/S0092-8674(00)80059-8)
- Gandy, K.A., D. Canals, M. Adada, M. Wada, P. Roddy, A.J. Snider, Y.A. Hannun, and L.M. Obeid. 2013. Sphingosine 1-phosphate induces filopodia formation through S1PR2 activation of ERM proteins. *Biochem. J.* 449:661–672. <https://doi.org/10.1042/BJ20120213>
- Gary, R., and A. Bretscher. 1995. Ezrin self-association involves binding of an N-terminal domain to a normally masked C-terminal domain that includes the F-actin binding site. *Mol. Biol. Cell*. 6:1061–1075. <https://doi.org/10.1091/mbc.6.8.1061>
- Gilden, J.K., S. Peck, Y.-C.M. Chen, and M.F. Krummel. 2012. The septin cytoskeleton facilitates membrane retraction during motility and blebbing. *J. Cell Biol.* 196:103–114. <https://doi.org/10.1083/jcb.201105127>
- Grayson, M.H., R.S. Hotchkiss, I.E. Karl, M.J. Holtzman, and D.D. Chaplin. 2003. Intravital microscopy comparing T lymphocyte trafficking to the spleen and the mesenteric lymph node. *Am. J. Physiol. Heart Circ. Physiol.* 284:H2213–H2226. <https://doi.org/10.1152/ajpheart.00999.2002>
- Grigorova, I.L., S.R. Schwab, T.G. Phan, T.H.M. Pham, T. Okada, and J.G. Cyster. 2009. Cortical sinus probing, S1P1-dependent entry and flow-based capture of egressing T cells. *Nat. Immunol.* 10:58–65. <https://doi.org/10.1038/ni.1682>
- Hayashi, K., S. Yonemura, T. Matsui, and S. Tsukita. 1999. Immunofluorescence detection of ezrin/radixin/moesin (ERM) proteins with their carboxyl-terminal threonine phosphorylated in cultured cells and tissues. *J. Cell Sci.* 112:1149–1158.
- Hirata, T., A. Nomachi, K. Tohya, M. Miyasaka, S. Tsukita, T. Watanabe, and S. Narumiya. 2012. Moesin-deficient mice reveal a non-redundant role for moesin in lymphocyte homeostasis. *Int. Immunol.* 24:705–717. <https://doi.org/10.1093/intimm/dxs077>
- Ikebe, M., J. Koretz, and D.J. Hartshorne. 1988. Effects of phosphorylation of light chain residues threonine 18 and serine 19 on the properties and conformation of smooth muscle myosin. *J. Biol. Chem.* 263:6432–6437. [https://doi.org/10.1016/S0021-9258\(18\)68804-0](https://doi.org/10.1016/S0021-9258(18)68804-0)
- Jacobelli, J., R.S. Friedman, M.A. Conti, A.-M. Lennon-Dumenil, M. Piel, C.M. Sorensen, R.S. Adelstein, and M.F. Krummel. 2010. Confinement-optimized three-dimensional T cell amoeboid motility is modulated



- via myosin IIA-regulated adhesions. *Nat. Immunol.* 11:953–961. <https://doi.org/10.1038/ni.1936>
- Jacobelli, J., M. Estin Matthews, S. Chen, and M.F. Krummel. 2013. Activated T cell trans-endothelial migration relies on myosin-IIA contractility for squeezing the cell nucleus through endothelial cell barriers. *PLoS One* 8: e75151. <https://doi.org/10.1371/journal.pone.0075151>
- Jalkanen, S., and M. Salmi. 2020. Lymphatic endothelial cells of the lymph node. *Nat. Rev. Immunol.* 20:566–578. <https://doi.org/10.1038/s41577-020-0281-x>
- Lagresle-Peyrou, C., S. Luce, F. Ouchani, T.S. Soheili, H. Sadek, M. Chouteau, A. Durand, I. Pic, J. Majewski, C. Brouzes, et al. 2016. X-linked primary immunodeficiency associated with hemizygous mutations in the moesin (MSN) gene. *J. Allergy Clin. Immunol.* 138:1681–1689.e8. <https://doi.org/10.1016/j.jaci.2016.04.032>
- Lämmermann, T., B.L. Bader, S.J. Monkley, T. Worbs, R. Wedlich-Söldner, K. Hirsch, M. Keller, R. Förster, D.R. Critchley, R. Fässler, and M. Sixt. 2008. Rapid leukocyte migration by integrin-independent flowing and squeezing. *Nature*. 453:51–55. <https://doi.org/10.1038/nature06887>
- Liu, Y., N.V. Belkina, C. Park, R. Nambiar, S.M. Loughhead, G. Patino-Lopez, K. Ben-Aissa, J.-J. Hao, M.J. Kruhlak, H. Qi, et al. 2012. Constitutively active ezrin increases membrane tension, slows migration, and impedes endothelial transmigration of lymphocytes in vivo in mice. *Blood*. 119: 445–453. <https://doi.org/10.1182/blood-2011-07-368860>
- Lorentzen, A., J. Bamber, A. Sadok, I. Elson-Schwab, and C.J. Marshall. 2011. An ezrin-rich, rigid uropod-like structure directs movement of amoeboid blebbing cells. *J. Cell Sci.* 124:1256–1267. <https://doi.org/10.1242/jcs.074849>
- Lyons, A.B., and C.R. Parish. 1995. Are murine marginal-zone macrophages the splenic white pulp analog of high endothelial venules? *Eur. J. Immunol.* 25:3165–3172. <https://doi.org/10.1002/eji.1830251127>
- Mandl, J.N., R. Liou, F. Klauschen, N. Vrisekoop, J.P. Monteiro, A.J. Yates, A.Y. Huang, and R.N. Germain. 2012. Quantification of lymph node transit times reveals differences in antigen surveillance strategies of naive CD4+ and CD8+ T cells. *Proc. Natl. Acad. Sci. USA*. 109:18036–18041. <https://doi.org/10.1073/pnas.1211717109>
- Martinelli, S., E.J.H. Chen, F. Clarke, R. Lyck, S. Affentranger, J.K. Burkhardt, and V. Niggli. 2013. Ezrin/Radixin/Moesin proteins and flotillins cooperate to promote uropod formation in T cells. *Front. Immunol.* 4:84. <https://doi.org/10.3389/fimmu.2013.00084>
- Matloubian, M., C.G. Lo, G. Cinamon, M.J. Lesneski, Y. Xu, V. Brinkmann, M.L. Allende, R.L. Proia, and J.G. Cyster. 2004. Lymphocyte egress from thymus and peripheral lymphoid organs is dependent on SIP receptor 1. *Nature*. 427:355–360. <https://doi.org/10.1038/nature02284>
- Mori, K., M. Itoi, N. Tsukamoto, H. Kubo, and T. Amagai. 2007. The perivascular space as a path of hematopoietic progenitor cells and mature T cells between the blood circulation and the thymic parenchyma. *Int. Immunol.* 19:745–753. <https://doi.org/10.1093/intimm/dxm041>
- Mullershausen, F., F. Zecri, C. Cetin, A. Billich, D. Guerini, and K. Seuwen. 2009. Persistent signaling induced by FTY720-phosphate is mediated by internalized SIP1 receptors. *Nat. Chem. Biol.* 5:428–434. <https://doi.org/10.1038/nchembio.173>
- Nicosia, M., S. Miyairi, A. Beavers, G.W. Farr, P.R. McGuirk, M.F. Pelletier, and A. Valujskikh. 2019. Aquaporin 4 inhibition alters chemokine receptor expression and T cell trafficking. *Sci. Rep.* 9:7417. <https://doi.org/10.1038/s41598-019-43884-2>
- Nomachi, A., M. Yoshinaga, J. Liu, P. Kanchanawong, K. Tohyama, D. Thumkeo, T. Watanabe, S. Narumiya, and T. Hirata. 2013. Moesin controls clathrin-mediated SIPR1 internalization in T cells. *PLoS One* 8: e82590. <https://doi.org/10.1371/journal.pone.0082590>
- Ohl, L., G. Bernhardt, O. Pabst, and R. Förster. 2003. Chemokines as organizers of primary and secondary lymphoid organs. *Semin. Immunol.* 15: 249–255. <https://doi.org/10.1016/j.smim.2003.08.003>
- Pappu, R., S.R. Schwab, I. Cornelissen, J.P. Pereira, J.B. Regard, Y. Xu, E. Camerer, Y.-W. Zheng, Y. Huang, J.G. Cyster, and S.R. Coughlin. 2007. Promotion of lymphocyte egress into blood and lymph by distinct sources of sphingosine-1-phosphate. *Science*. 316:295–298. <https://doi.org/10.1126/science.1139221>
- Parameswaran, N., K. Matsui, and N. Gupta. 2011. Conformational switching in ezrin regulates morphological and cytoskeletal changes required for B cell chemotaxis. *J. Immunol.* 186:4088–4097. <https://doi.org/10.4049/jimmunol.1001139>
- Petrie, R.J., and H. Koo. 2014. Direct measurement of intracellular pressure. *Curr. Protoc. Cell Biol.* 63:12.9.1–12.9.9. <https://doi.org/10.1002/0471143030.cb1209s63>
- Pflicke, H., and M. Sixt. 2009. Preformed portals facilitate dendritic cell entry into afferent lymphatic vessels. *J. Exp. Med.* 206:2925–2935. <https://doi.org/10.1084/jem.20091739>
- Schwab, S.R., J.P. Pereira, M. Matloubian, Y. Xu, Y. Huang, and J.G. Cyster. 2005. Lymphocyte sequestration through SIP lyase inhibition and disruption of SIP gradients. *Science*. 309:1735–1739. <https://doi.org/10.1126/science.1113640>
- Shaffer, M.H., R.S. Dupree, P. Zhu, I. Saotome, R.F. Schmidt, A.I. McClatchey, B.D. Freedman, and J.K. Burkhardt. 2009. Ezrin and moesin function together to promote T cell activation. *J. Immunol.* 182:1021–1032. <https://doi.org/10.4049/jimmunol.182.2.1021>
- Shapiro, L., A.M. Fannon, P.D. Kwong, A. Thompson, M.S. Lehmann, G. Grubel, J.-F. Legrand, J. Als-Nielsen, D.R. Colman, and W.A. Hendrickson. 1995. Structural basis of cell-cell adhesion by cadherins. *Nature*. 374:327–337. <https://doi.org/10.1038/374327a0>
- Smith, M.E., and W.L. Ford. 1983. The recirculating lymphocyte pool of the rat: a systematic description of the migratory behaviour of recirculating lymphocytes. *Immunology*. 49:83–94.
- Stroka, K.M., H. Jiang, S.H. Chen, Z. Tong, D. Wirtz, S.X. Sun, and K. Konstantopoulos. 2014. Water permeation drives tumor cell migration in confined microenvironments. *Cell*. 157:611–623. <https://doi.org/10.1016/j.cell.2014.02.052>
- Strychalski, W., and R.D. Guy. 2016. Intracellular Pressure Dynamics in Blebbing Cells. *Biophys. J.* 110:1168–1179. <https://doi.org/10.1016/j.bpj.2016.01.012>
- Teo, G.S.L., J.A. Ankrum, R. Martinelli, S.E. Boetto, K. Simms, T.E. Sciuto, A.M. Dvorak, J.M. Karp, and C.V. Carman. 2012. Mesenchymal stem cells transigrate between and directly through tumor necrosis factor- $\alpha$ -activated endothelial cells via both leukocyte-like and novel mechanisms. *Stem Cells*. 30:2472–2486. <https://doi.org/10.1002/stem.1198>
- Tinevez, J.-Y., U. Schulze, G. Salbreux, J. Roensch, J.-F. Joanny, and E. Paluch. 2009. Role of cortical tension in bleb growth. *Proc. Natl. Acad. Sci. USA*. 106:18581–18586. <https://doi.org/10.1073/pnas.0903353106>
- Tooley, A.J., J. Gilden, J. Jacobelli, P. Beemiller, W.S. Trimble, M. Kinoshita, and M.F. Krummel. 2009. Amoeboid T lymphocytes require the septin cytoskeleton for cortical integrity and persistent motility. *Nat. Cell Biol.* 11:17–26. <https://doi.org/10.1038/ncb1808>
- Tozluoglu, M., A.L. Tourmier, R.P. Jenkins, S. Hooper, P.A. Bates, and E. Sahai. 2013. Matrix geometry determines optimal cancer cell migration strategy and modulates response to interventions. *Nat. Cell Biol.* 15: 751–762. <https://doi.org/10.1038/ncb2775>
- Umemoto, S., A.R. Bengur, and J.R. Sellers. 1989. Effect of multiple phosphorylations of smooth muscle and cytoplasmic myosins on movement in an in vitro motility assay. *J. Biol. Chem.* 264:1431–1436. [https://doi.org/10.1016/S0021-9258\(18\)94205-5](https://doi.org/10.1016/S0021-9258(18)94205-5)
- Viswanatha, R., J. Wayt, P.Y. Ohouo, M.B. Smolka, and A. Bretscher. 2013. Interactome analysis reveals ezrin can adopt multiple conformational states. *J. Biol. Chem.* 288:35437–35451. <https://doi.org/10.1074/jbc.M113.505669>
- Vrzalikova, K., M. Ibrahim, M. Vockerodt, T. Perry, S. Margielewska, L. Lupino, E. Nagy, E. Soilleux, D. Liebelt, R. Hollows, et al. 2018. SIPR1 drives a feedforward signalling loop to regulate BATF3 and the transcriptional programme of Hodgkin lymphoma cells. *Leukemia*. 32: 214–223. <https://doi.org/10.1038/leu.2017.275>
- Wendt, T., D. Taylor, K.M. Trybus, and K. Taylor. 2001. Three-dimensional image reconstruction of dephosphorylated smooth muscle heavy meromyosin reveals asymmetry in the interaction between myosin heads and placement of subfragment 2. *Proc. Natl. Acad. Sci. USA* 98: 4361–4366. <https://doi.org/10.1073/pnas.071051098>
- Willinger, T., S.M. Ferguson, J.P. Pereira, P. De Camilli, and R.A. Flavell. 2014. Dynamin 2-dependent endocytosis is required for sustained SIPR1 signaling. *J. Exp. Med.* 211:685–700. <https://doi.org/10.1084/jem.20131343>
- Xiong, Y., W. Piao, C.C. Brinkman, L. Li, J.M. Kulinski, A. Olivera, A. Cartier, T. Hla, K.L. Hippen, B.R. Blazar, et al. 2019. CD4 T cell sphingosine 1-phosphate receptor (SIPR)1 and SIPR4 and endothelial SIPR2 regulate afferent lymphatic migration. *Sci. Immunol.* 4:eaa1263. <https://doi.org/10.1126/sciimmunol.aav1263>
- Yatomi, Y., Y. Igarashi, L. Yang, N. Hisano, R. Qi, N. Asazuma, K. Satoh, Y. Ozaki, and S. Kume. 1997. Sphingosine 1-phosphate, a bioactive sphingolipid abundantly stored in platelets, is a normal constituent of human plasma and serum. *J. Biochem.* 121:969–973. <https://doi.org/10.1093/oxfordjournals.jbchem.a021681>
- Zachariah, M.A., and J.G. Cyster. 2010. Neural crest-derived pericytes promote egress of mature thymocytes at the corticomedullary junction. *Science*. 328:1129–1135. <https://doi.org/10.1126/science.1188222>
- Zatulovskiy, E., R. Tyson, T. Bretschneider, and R.R. Kay. 2014. Bleb-driven chemotaxis of Dictyostelium cells. *J. Cell Biol.* 204:1027–1044. <https://doi.org/10.1083/jcb.201306147>

## Supplemental material

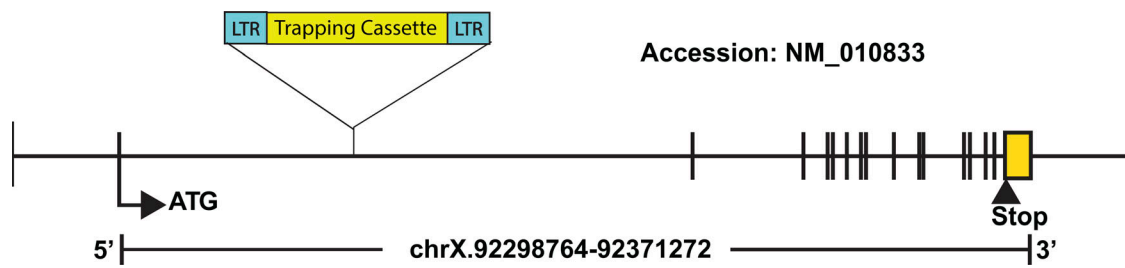


Figure S1. **Schematic of the *Msn* targeting strategy.** The diagram shows the insertion of the trapping cassette into the first intron of the *Msn* gene in 129/Sv ES clones (OST432827), which were used to generate the mice used in this report. The accession number [NM\\_010833](https://www.ncbi.nlm.nih.gov/nuccore/NM_010833) is from the Reference Sequence database.

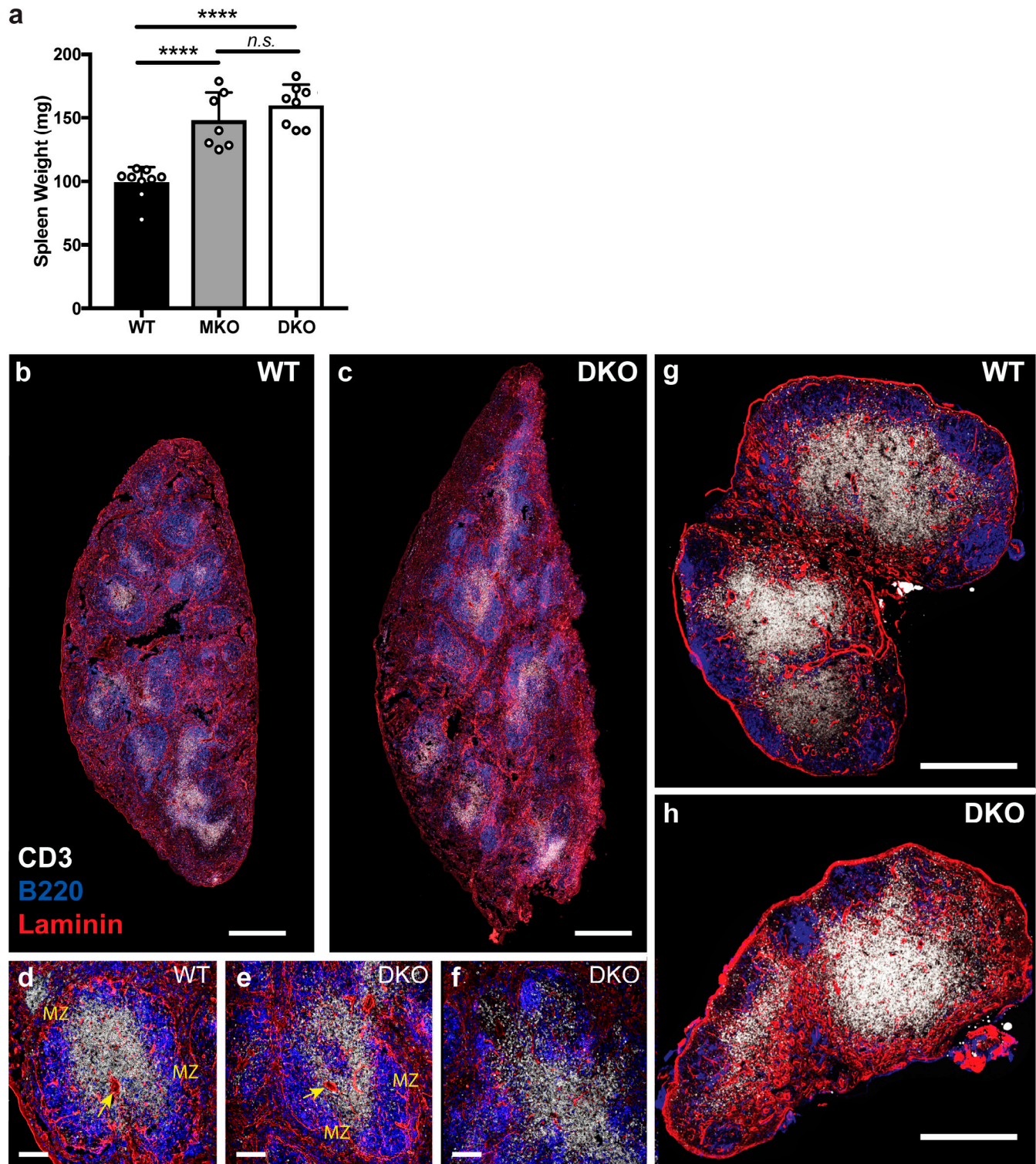


Figure S2. **Organization of secondary lymphoid organs in DKO mice.** **(a)** Weight of spleens isolated from WT, MKO, and DKO mice. Data are displayed as means  $\pm$  SD. Each dot corresponds to an individual mouse;  $n = 7-9$  mice per group. Means were compared using an ordinary one-way ANOVA. Data distribution was assumed to be normal, but this was not formally tested. **(b-h)** Immunofluorescence histology of spleens and lymph nodes from WT and DKO mice stained with antibodies against CD3 (white), B220 (blue), and laminin (red). **(b and c)** Confocal tile scans of whole spleens from WT and DKO mice; scale bar, 500  $\mu$ m. **(d-f)** Magnified regions of spleens with the central arterioles (arrows) and marginal zones (MZ) labeled. Normal lymphocyte organization in WT and DKO spleens shown (d and e) as well as a representative region of poor organization in DKO spleen (f). Scale bar, 100  $\mu$ m. **(g and h)** Confocal tile scans of whole inguinal lymph nodes from WT and DKO mice. Scale bar, 500  $\mu$ m. n.s.,  $P > 0.05$ ; \*\*\*\*,  $P < 0.0001$ .

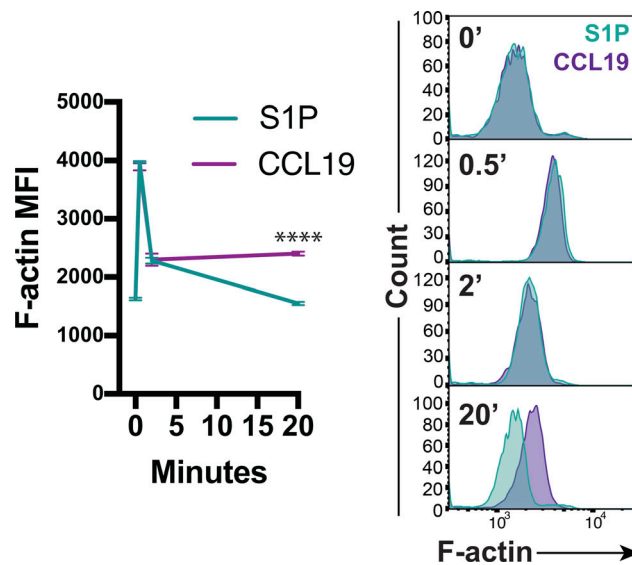
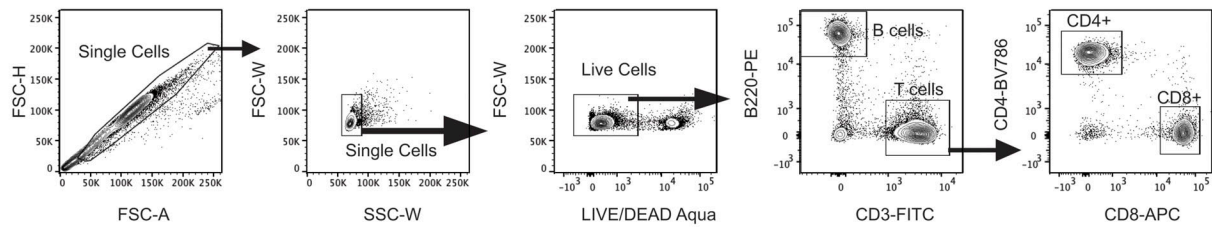
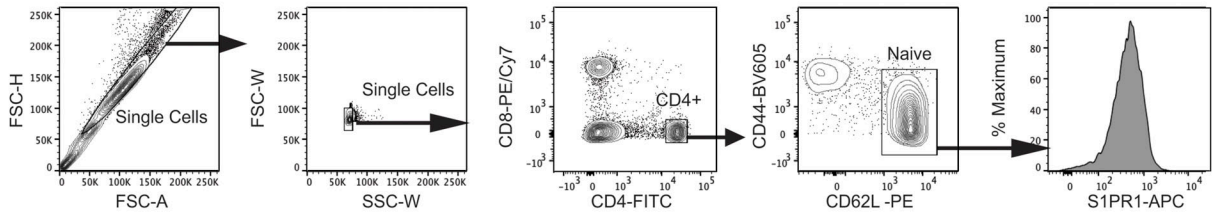


Figure S3. **Actin polymerization kinetics for S1P versus chemokine stimulation.** WT naive CD4<sup>+</sup> T cells cultured overnight were stimulated with S1P (1 nM) or CCL19 (100 ng/ml), fixed after 0, 0.5, 2, or 20 min, stained for F-actin, and analyzed by flow cytometry. Representative plots (gated on CD4<sup>+</sup> singlets) and pooled data from three independent experiments shown as means  $\pm$  SD and compared at each time point using multiple *t* tests (two-sided) with the Holm-Sidak correction for multiple comparisons. Data distribution was assumed to be normal, but this was not formally tested. MFI, mean fluorescence intensity. \*\*\*\*,  $P < 0.0001$ .

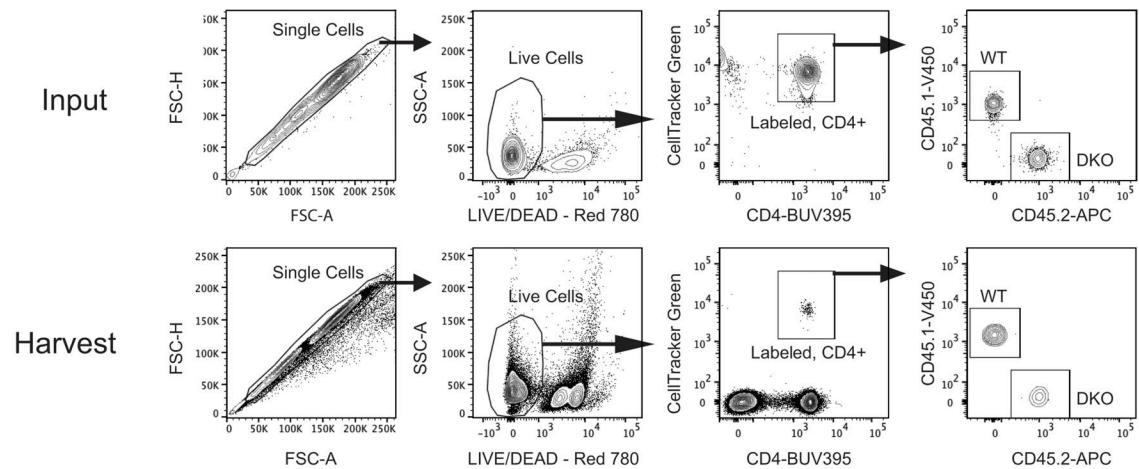
### a Mouse Characterization



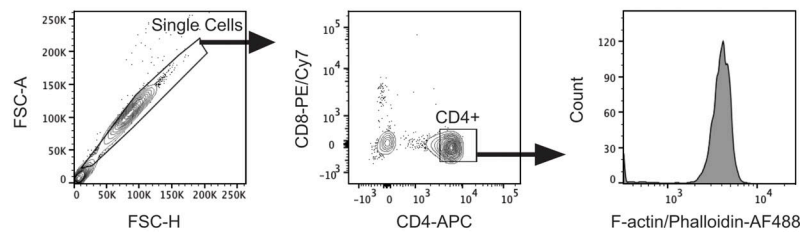
### b Naive CD4<sup>+</sup> T cell S1PR1 Surface Expression, *ex vivo*



### c Competitive *in vivo* Migration



### d Actin Polymerization Assays



### e S1PR1 Endocytosis Assays

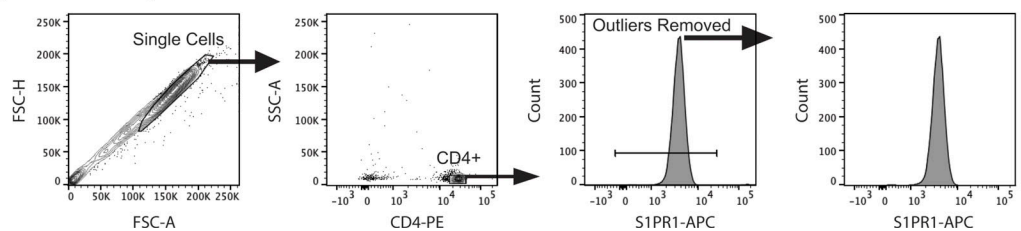


Figure S4. **Flow cytometry gating strategies.** (a) For mouse characterization studies (Fig. 1), cell suspensions prepared from the lymphoid organs or blood were gated on single cells and live cells, then the indicated lineage-defining surface markers. (b) Gating on naive CD4<sup>+</sup> T cells to determine surface S1PR1 expression, corresponds to Fig. 4 a. (c) Gating showing the mixed population of CellTracker Green-labeled WT (CD45.1<sup>+</sup>) and DKO (CD45.2<sup>+</sup>) T cells. Input refers to what was injected into recipient animals; harvest refers to lymphoid organs and blood harvested 1 or 24 h later. Corresponds to Fig. 2, g and h. (d) Gating on singlets and CD4<sup>+</sup>CD8<sup>-</sup> T cells for actin polymerization studies. Note that the fixation strategy used in these studies precludes live/dead staining. (e) Gating on singlet CD4<sup>+</sup> cells for *in vitro* S1PR1 endocytosis studies. Small amounts of extremely high S1PR1<sup>+</sup> cells that skewed quantitation and were later confirmed to be dead cells were gated out. FSC-A, forward scatter area; FSC-H, forward scatter height; FSC-W, forward scatter width; SSC-W, side scatter width.

Video 1. **WT T cells undergoing S1P-induced chemokinesis.** WT naive CD4<sup>+</sup> T cells were allowed to settle on VCAM-coated coverslips for 30 min at 37°C. Cells were imaged by DIC microscopy using a 63× objective. Images were captured every second for 2 min, at which point S1P (100 nM final) was gently dripped into the chamber. Imaging was continued for an additional 7 min. The playback rate is 40 frames per second (40×), and the indicated time (min:s) is relative to S1P stimulation.

Video 2. **WT T cells undergoing CCL19-induced chemokinesis.** WT naive CD4<sup>+</sup> T cells were allowed to settle on VCAM-coated coverslips for 30 min at 37°C. Cells were imaged by DIC microscopy using a 63× objective. Images were captured every second for 2 min, at which point CCL19 (100 µg/ml final) was gently dripped into the chamber. Imaging was continued for an additional 7 min. The playback rate is 40 frames per second (40×), and the indicated time (min:s) is relative to CCL19 stimulation.

Video 3. **WT T cells undergoing CXCL12-induced chemokinesis.** WT naive CD4<sup>+</sup> T cells were allowed to settle on VCAM-coated coverslips for 30 min at 37°C. Cells were imaged by DIC microscopy using a 63× objective. Images were captured every second for 2 min, at which point CXCL12 (100 µg/ml final) was gently dripped into the chamber. Imaging was continued for an additional 7 min. The playback rate is 40 frames per second (40×), and the indicated time (min:s) is relative to CXCL12 stimulation.

Video 4. **DKO T cells undergoing S1P-induced chemokinesis.** DKO naive CD4<sup>+</sup> T cells were allowed to settle on VCAM-coated coverslips for 30 min at 37°C. Cells were imaged by DIC microscopy using a 63× objective. Images were captured every second for 2 min, at which point S1P (100 nM final) was gently dripped into the chamber. Imaging was continued for an additional 7 min. The playback rate is 40 frames per second (40×), and the indicated time (min:s) is relative to S1P stimulation.

Video 5. **Lamellipodia to bleb transition, example 1.** WT naive CD4<sup>+</sup> T cells were stimulated and imaged exactly as in [Video 1](#). The arrow indicates the cell of interest; asterisks denote blebs. The playback rate is 6 frames per second (6×). The indicated time (min:s) is relative to S1P stimulation.

Video 6. **Lamellipodia to bleb transition, example 2.** WT naive CD4<sup>+</sup> T cells were stimulated and imaged exactly as in [Video 1](#). The arrow indicates the cell of interest; asterisks denote blebs. The playback rate is 6 frames per second (6×). The indicated time (min:s) is relative to S1P stimulation.

Video 7. **DKO T cell blebbing, example showing poor displacement.** DKO naive CD4<sup>+</sup> T cells were stimulated and imaged exactly as in [Video 4](#). The arrow indicates the cell of interest; asterisks denote blebs. The playback rate is 6 frames per second (6×). The indicated time (min:s) is relative to S1P stimulation.

Video 8. **DKO T cell blebbing, example showing poor directionality.** DKO naive CD4<sup>+</sup> T cells were stimulated and imaged exactly as in [Video 4](#). The arrow indicates the cell of interest; asterisks denote blebs. The playback rate is 6 frames per second (6×). The indicated time (min:s) is relative to S1P stimulation.